RSMC Tokyo – Typhoon Center

Technical Review

No. 11

Contents

Japan Meteorological Agency

March 2009

PREFACE

The RSMC Tokyo - Typhoon Center provides various tropical cyclone information products to National Meteorological and Hydrological Services (NMHSs) on a real-time basis in order to support tropical cyclone forecasting as well as disaster preparedness and prevention activities. The Center also offers publications such as *RSMC Tropical Cyclone Best Track* and *Annual Report on the Activities of the RSMC Tokyo - Typhoon Center* every year. In addition to these regular publications, the Center occasionally publishes *Technical Review* to outline the achievements of research and development on operational meteorological services for tropical cyclones.

This issue of *Technical Review No. 11* covers three topics relating to numerical prediction models and storm surge prediction. These are: 1) Outline of the High Resolution Global Model at the Japan Meteorological Agency, 2) Outline of the Typhoon Ensemble Prediction System at the Japan Meteorological Agency, and 3) Outline of the Storm Surge Prediction Model at the Japan Meteorological Agency. The first of these explains the upgraded Global Spectral Model and its performance in TC track and intensity forecasts. The second describes a new Ensemble Prediction System that JMA began to operate for improving TC track forecasts. The third topic explains a numerical storm surge model to provide the basis for issuing storm surge warnings.

The RSMC Tokyo - Typhoon Center hopes this issue will serve as a useful reference to the understanding of typhoon forecast with NWP and the mitigation of typhoon-related disasters.

Outline of the High Resolution Global Model at the Japan Meteorological Agency

Masayuki Nakagawa
Numerical Prediction Division, Japan Meteorological Agency

Abstract

The Japan Meteorological Agency (JMA) upgraded the resolution of the Global Spectral Model (GSM) from TL319L40 to TL959L60 on 21 November 2007, when the Typhoon Model retired from operational use. Since then, tropical cyclone (TC) track and intensity forecasts have been supported by GSM only. GSM provides numerical weather prediction (NWP) products four times a day for all TCs existing globally. This paper gives an outline of the high resolution GSM and shows its performance in TC track and intensity forecasts.

1. Introduction

The Japan Meteorological Agency (JMA) provides a variety of numerical weather prediction (NWP) products that play a vital role in both national and international weather services. Among these, tropical cyclone (TC) track and intensity forecasts are the most important for disaster prevention and preparedness activities.

On 21 November 2007, the spatial resolution of the Global Spectral Model (GSM) was greatly enhanced from the previous TL319L40 (approximately 60 km in the horizontal and 40 layers up to 0.4 hPa in the vertical) to TL959L60 (approximately 20 km in the horizontal and 60 layers up to 0.1 hPa in the vertical) (Iwamura and Kitagawa 2008). Until that time, JMA had operated not only GSM (TL319L40) but also the 24-km resolution Typhoon Model (TYM), covering a TC and its surrounding areas to provide TC track and intensity forecasts. TYM had been run for two TCs at most for each initial time. Since the time of the increase of the resolution of GSM, when TYM retired from operational use, TC forecasts have been supported only by GSM covering the entire globe. GSM provides high resolution NWP products four times a day for all TCs worldwide.

In February 2008, JMA began the operation of a TC ensemble prediction system (the Typhoon Ensemble Prediction System, or TEPS) to improve both deterministic and probabilistic forecasts of TC movements after a period of preliminary operation from May 2007. For details of TEPS, see Yamaguchi and Komori (2009).

This paper describes the high resolution global NWP system. Section 2 introduces the major features and specifications of GSM. Section 3 gives examples and statistical scores of typhoon track

and intensity forecasts. A summary of the results and conclusions are presented in section 4.

2. Outline of the global NWP system

The specifications of the previous GSM, TYM, current GSM and TEPS are summarized in Table 1. The major changes made to GSM in November 2007 are as follows:

- an increase in the resolution from TL319L40 to TL959L60 with the topmost level raised from 0.4 hPa to 0.1 hPa,
- an increase in the resolution of the inner model of the four-dimensional variational (4D-Var) data assimilation system from T106L40 to T159L60,
- use of data from new high resolution analysis of sea surface temperature and sea ice concentration as ocean surface boundary conditions,
- use of surface snow depth data from the domestic dense observational network in global snow depth analysis,
- upgrade of the numerical integration scheme from a three-time-level leap-frog scheme to a two-time-level scheme,
- introduction of a new convective triggering scheme proposed by Xie and Zhang (2000) into the deep convection parameterization, and
- introduction of a new two-dimensional aerosol climatology derived from satellite observations for the radiation calculation.

Table 1 Framework of previous and current NWP models for TC forecasts at JMA

	Global Model (GSM, previous)	Typhoon Model (TYM, terminated)	Global Model (GSM, current)	Typhoon Ensemble Prediction System (TEPS)
Forecast domain	Global	TC and its surrounding areas	Global	
Grid size / Number of grids	0.5625 deg. / 640 x 320 (TL319)	24 km / 271 x 271	0.1875 deg. / 1920 (equator) – 6 deg. / 60 (closest to pole) x 960 (TL959)	0.5625 deg. / 640 x 320 (TL319)
Vertical levels / Top	40 / 0.4 hPa	25 / 17.5 hPa	60 / 0.1 hPa	
Forecast range (initial time)	90 hours (00UTC), 216 hours (12 UTC), 36 hours (06, 18 UTC)	84 hours (00, 06, 12, 18 UTC) Maximum 2 runs for each initial time	84 hours (00, 06, 18 UTC), 216 hours (12 UTC)	132 hours (00, 06, 12, 18 UTC) 11 members
Analysis	4D-Var	Global analysis	4D-Var	Global analysis with SV ensemble perturbations

For the global analysis, 4D-Var data assimilation method is employed. The control variables are relative vorticity, unbalanced divergence, unbalanced temperature, unbalanced surface pressure and the natural logarithm of specific humidity. In order to improve computational efficiency, an incremental method is adopted in which the analysis increment is first evaluated at a lower horizontal resolution (T159) before being interpolated and added to the first-guess field at the original resolution (TL959). The specifications of the atmospheric analysis schemes are listed in Table 2.

Global analyses are performed at 00, 06, 12 and 18 UTC every day. An early analysis with a short cut-off time is performed to prepare the initial conditions for operational forecast, and a cycle analysis with a long cut-off time is performed to pursue better quality of the global data assimilation system.

For TCs in the western North Pacific, typhoon bogus data are generated and assimilated for each TC to represent the structure accurately in the initial field for the forecast models. These consist of data relating to the artificial sea-surface pressure, temperature and wind data encircling each TC. The structure is axi-asymmetric. At first, a symmetric bogus profile is automatically generated based on the central pressure and 30-kt wind speed radius of the TC analyzed by forecasters. An axi-asymmetric bogus profile is then generated by retrieving asymmetric components from the first-guess field. The symmetric and axi-asymmetric profiles are combined to form the final bogus profile, which is then converted into pseudo-observation data for use in the global analysis.

GSM employs hydrostatic primitive equations with a shallow atmosphere assumption to express the resolvable motions and states of the atmosphere. The prognostic variables are wind (zonal and meridional), temperature, specific humidity, surface pressure and cloud water content. In

Table 2 Specifications of global objective analysis

Cut-off time	2 hr 20 min for early run analyses at 00, 06, 12 and 18 UTC, 11 hr 35 min for cycle run analyses at 00 and 12 UTC, 5 hr 35 min for cycle run analyses at 06 and 18 UTC
First guess	6-hour forecast by GSM
Grid form, resolution and number of grids	Reduced Gaussian grid, 0.1875-6 deg.,1920-60 x 960 for outer model Standard Gaussian grid, 0.75 deg., 480 x 240 for inner model
Levels	60 forecast model levels up to 0.1 hPa + surface
Analysis variables	Wind, surface pressure, temperature and specific humidity
Methodology	4D-Var scheme on model levels
Data used	SYNOP, SHIP, BUOY, TEMP, PILOT, Wind Profiler, AIREP, radiances from NOAA/ATOVS, MetOp/ATOVS, Aqua/AMSU-A, clear-sky radiances and atmospheric motion vectors (AMVs) from MTSAT-1R, GOES, METEOSAT, MODIS polar AMVs, SeaWinds, Microwave imager radiometer radiances (AMSR-E, TMI, SSM/I) and Australian PAOB; Typhoon bogussing applied for analysis
Initialization	Non-linear normal mode initialization for inner model

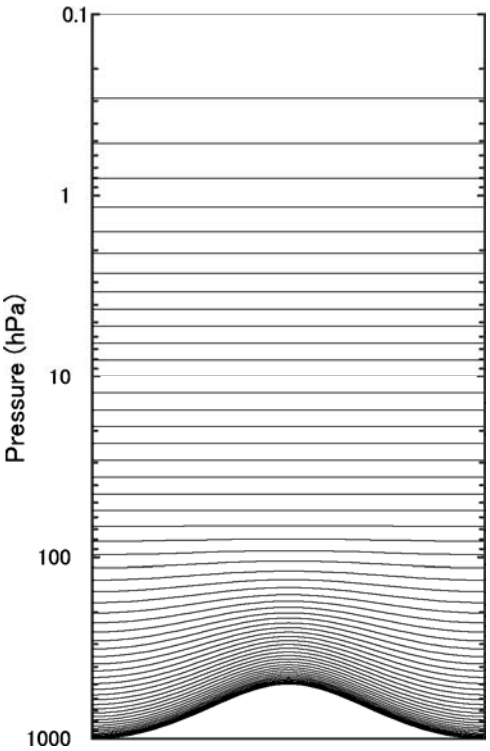

Figure 1 Distribution of vertical layers of GSM

the horizontal, the prognostic variables are spectrally discretized with a triangular truncation wave of 959 (TL959). The corresponding transform grids are spaced by about 0.1875 degrees representing about 20 km. Such high resolution enables detailed representation of land/sea mask and topography, which could improve forecasts of synoptic and sub-synoptic weather. In the vertical, a sigma-p hybrid coordinate is introduced. GSM has 60 layers up to 0.1 hPa as shown in Figure 1. The vertical resolution is higher in the lower atmosphere for better simulation of the planetary boundary layer processes. The raised topmost level helps to assimilate satellite observations more effectively.

The time integration is based on a two-time-level, semi-implicit semi-Lagrangian scheme. A vertically conservative semi-Lagrangian scheme (Yoshimura and Matsumura 2003) is adopted and fourth-order linear horizontal diffusion is applied. GSM also includes sophisticated parameterization schemes for physical processes such as gravity wave drag, planetary boundary layer, land surface, radiation, cumulus convection and cloud. JMA runs GSM four times a day (84-hour forecasts from 00, 06 and 18 UTC and 216-hour forecasts from 12 UTC). The specifications of GSM are listed in Table 3.

In January 2008, JMA revised the calculation procedure for the convective triggering mechanism in GSM to accurately consider the effect of wind crossing isobars at the surface, which had not been calculated correctly in the previous version (Nakagawa 2008). Excessive limitation of cumulus upward mass flux from a redundant vertical CFL condition was also removed.

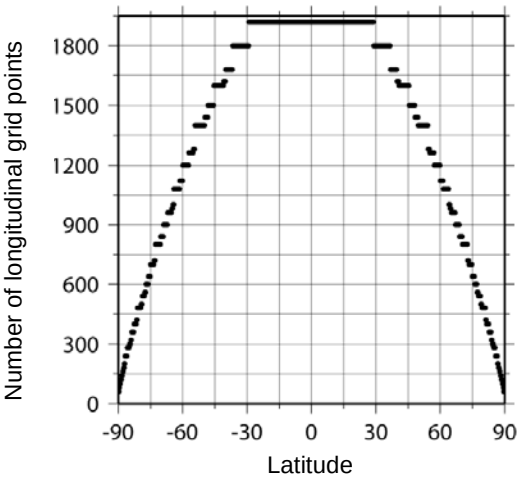

Figure 2 Number of longitudinal grid points against latitude in reduced Gaussian grid GSM (TL959)

In August 2008, a reduced Gaussian grid was implemented in GSM as a new dynamical core (Miyamoto 2006). On the standard Gaussian grid, the longitudinal interval between neighboring grid points decreases as the latitude increases. Hence, it is redundant to use an equal number of grid points for all given latitudes in a global model. The introduction of the reduced Gaussian grid removes

Table 3　Specifications of GSM

Basic equation	Primitive equations
Independent variables	Latitude, longitude and sigma-pressure hybrid coordinates and time
Dependent variables	Winds (zonal, meridional), temperature, specific humidity, surface pressure and cloud water content
Numerical technique	Spectral (spherical harmonics basis functions) in the horizontal Finite differences in the vertical Two-time-level, semi-Lagrangian, semi-implicit time integration scheme Hydrostatic approximation
Integration domain	Global in the horizontal Surface to 0.1 hPa in the vertical
Horizontal resolution	Spectral triangular 959 (TL959) roughly equivalent to 0.1875 x 0.1875 degrees lat-lon Reduced Gaussian grid, 1920 (equator) – 60 (pole) x 960
Vertical resolution	60 unevenly spaced sigma-p hybrid levels
Time step	10 minutes
Forecast time	84 hours from 00, 06 and 18 UTC, 216 hours from 12 UTC
Orography	GTOPO30 data set spectrally truncated and smoothed
Horizontal diffusion	Linear, fourth-order
Vertical diffusion	Stability (Richardson number) dependent, local formulation
Gravity wave drag	Longwave scheme (wavelengths > 100 km) mainly for stratosphere Shortwave scheme (wavelengths approx. 10 km) only for troposphere
Planetary boundary layer	Mellor and Yamada level-2 turbulence closure scheme Similarity theory in bulk formulae for surface layer
Treatment of sea surface	Climatological sea surface temperature with daily analyzed anomaly Climatological sea ice concentration with daily analyzed anomaly
Land surface	Simple Biosphere (SiB) model
Radiation	Two-stream with delta-Eddington approximation for shortwave Table look-up and k-distribution methods for longwave
Convection	Prognostic Arakawa-Schubert cumulus parameterization
Cloud	Prognostic cloud water, cloud cover diagnosed from moisture and cloud water

this redundancy by cutting grid points as shown in Figure 2, thus saving on computational resources. JMA is planning to introduce the reduced Gaussian grid to TEPS in the near future.

NWP products such as facsimile charts and Grid Point Value (GPV) data are disseminated through the JMA radio facsimile broadcast (JMH), the Global Telecommunication System (GTS), the RSMC Tokyo Data Serving System (RSMC DSS) and the World Meteorological Organization (WMO) Distributed Data Bases (DDBs) project server. Details of the NWP products disseminated are presented in the appendix.

3. Forecast of TC

3.1 Experimental design

In order to evaluate the forecast skill of the NWP system, forecast/assimilation experiments for TL959L60 GSM (August 2008 version with reduced Gaussian grid) and TL319L40 GSM (previous operational model) were conducted for August 2006 and January 2007. Starting from cycle analyses, 84-hour forecasts and 216-hour forecasts were performed with daily initiation at 00 UTC and 12 UTC, respectively. The forecasts of TCs in the responsibility area of the RSMC Tokyo - Typhoon Center (0°-60°N, 100°-180°E) were verified against the best track analyzed by the Center. The verified elements were the 84-hour forecasts of the center position, central pressure and maximum sustained winds. The results were compared to those of the operational TYM. In the statistical verification, samples in which all models were able to keep track of TCs were selected. It should be noted that the operational TYM started from initial fields based on early analysis of the operational TL319L40 GSM and used lateral boundary conditions interpolated from operational TL319L40 GSM forecasts starting from early analysis. As a result, the numbers of observation data used to make the TYM initial fields and lateral boundary conditions were less than those used to make the initial fields in the forecast/assimilation experiments for GSM, which may negatively affect the forecast skill of TYM.

3.2 Case study

Figure 3 shows the forecast track, central pressure and maximum sustained wind speed of Typhoon WUKONG (T0610) predicted by TL959L60 GSM, TL319L40 GSM and TYM along with the best track. The initial time of the forecasts is 12 UTC 16 August 2006. Moving to the northwest, WUKONG made landfall on Kyushu Island late on 17 August. After turning to the north, it weakened into a TD at 12UTC 19 August. TL959L60 GSM predicted the center position the best, while TL319L40 GSM and TYM showed westward and eastward error, respectively. As for the intensity of the typhoon, TL959L60 GSM could not sufficiently predict its weakening, which may be due to the poor representation of the effect of landfall. TL319L40 GSM predicted a weaker typhoon compared to the other models because of its low horizontal resolution. It was also unable to predict the weakening of the typhoon, due at least in part to it not making landfall on Kyushu Island. The typhoon predicted by TYM showed intensification in the early forecast hours. The tendency to predict larger development compared to TL959L60 GSM is a common feature in TYM forecast.

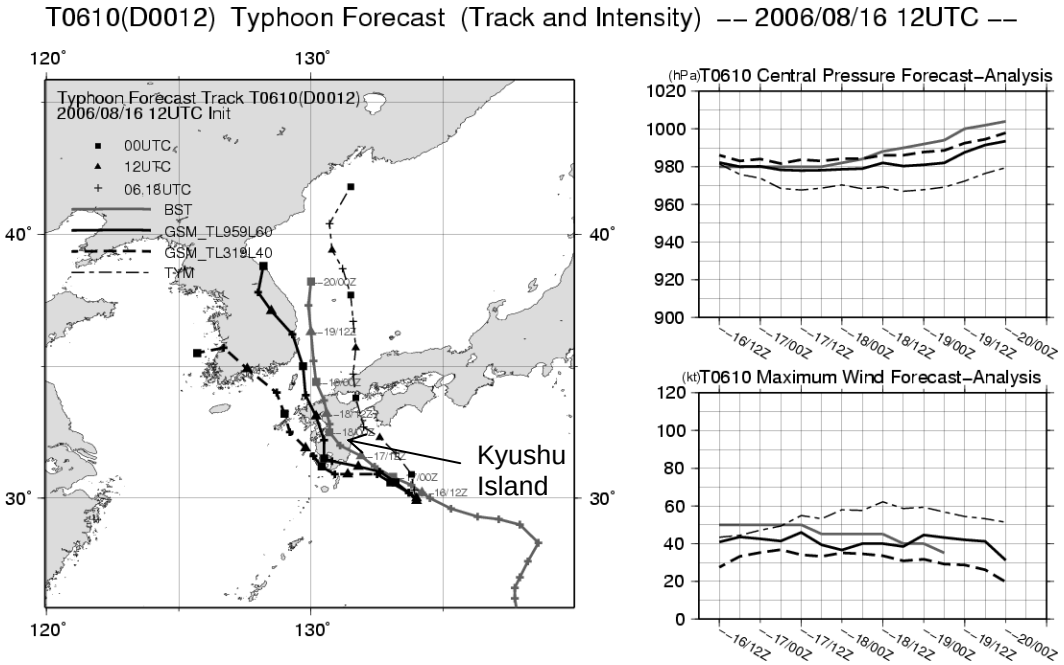

Figure 3 Predicted track (left), central pressure (top right) and maximum wind speed (bottom right) of T0610 (WUKONG). The initial time of the forecasts is 12 UTC 16 August 2006. The solid black line, broken black line, thin black dot-dash line and solid gray line indicate forecast by TL959L60 GSM, that by TL319L40 GSM, that by TYM and the analyzed best track, respectively.

The six-hour accumulated precipitations valid at 12 UTC 18 August 2006 in the forecasts by the three models and those analyzed are shown in Figure 4. The initial time of the forecasts is 12 UTC 17 August 2006, when Typhoon WUKONG was moving northward over Kyushu Island. All three models predicted the center position of the typhoon well in this case. Owing to its low horizontal resolution, TL319L40 GSM could not predict the detailed distribution of precipitation and strong rainfall over land caused by orographic effects. Although TYM represented orographic precipitation more strongly, its prediction of precipitation was too strong near the typhoon center and too weak away from the center. TL959L60 GSM simulated the distribution and intensity of precipitation better than other models, including orographic precipitation and heavy rainfall near the center of the

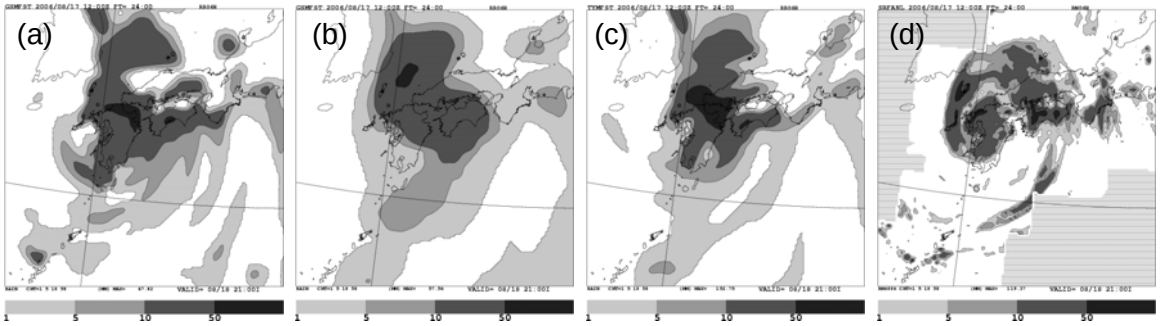

Figure 4 Six-hour accumulated precipitation valid at 12 UTC 18 August 2006. The initial time of the forecasts is 12 UTC 17 August 2006. (a): TL959L60 GSM forecast, (b): TL319L40 GSM forecast, (c): TYM forecast, (d): Radar-raingauge analysis. The gray horizontal lines in (d) indicate an absence of analysis.

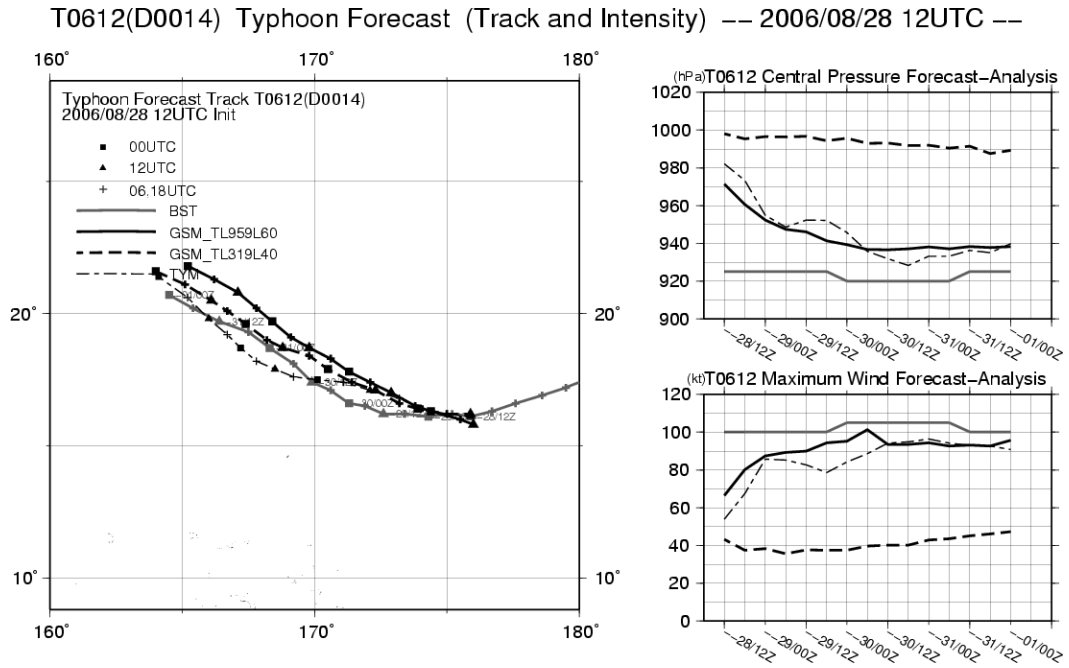

Figure 5 As Figure 3, but for T0612 (IOKE). The initial time of the forecasts is 12 UTC 28 August 2006.

typhoon.

Figure 5 shows the forecast track, central pressure and maximum sustained wind speed of Typhoon IOKE (T0612) predicted by the three models along with the best track. The initial time of the forecasts is 12 UTC 28 August 2006. IOKE turned to the west around the initial time and attained peak intensity with maximum sustained winds of 105 kt and a central pressure of 920 hPa over the sea southeast of Wake Island (16.3°N, 166.6°E) at 00 UTC 30 August. The difference between the typhoon track forecasts by the three models is relatively small, but the intensity forecasts vary widely. TL319L40 GSM predicted a rather weak typhoon compared to other models and the best track because of its low horizontal resolution. Higher resolution is needed for better representation of detailed structure of TCs, which is essential for realistic TC intensity forecasts. Meanwhile, TL959L60 GSM and TYM simulated the intensity of the typhoon fairly well as a whole, although a transient feature is seen in the early forecast hours. When generating the typhoon bogus data for the analysis, the typhoon central pressure is increased in most cases for adaptation to the horizontal resolution of the analysis to prevent the initial fields from being distorted by the extreme pressure gap between the inner and outer regions of the TC. This procedure may lead to the transient nature of the time evolution of error in typhoon intensity forecasts by TL959L60 GSM and TYM as seen in Figure 5. Furthermore, the typhoon bogus data is assimilated as observational data produced from the bogus structure in the global analysis, while the bogus structure itself is implanted directly into the first-guess fields in the analysis for TYM. This may also result in a shallower typhoon in the initial fields of TL959L60 GSM. However, it is not clear whether the typhoon represented by TL959L60 GSM and TYM in the early forecast hours is too weak or not. Further investigation is therefore needed on the depth to which a typhoon should be represented in NWP

models with a particular horizontal resolution such as 20 or 24 km. Nevertheless, it seems reasonable to say that TL959L60 GSM predicted the intensity of the typhoon as well as TYM in this case.

3.3 Statistics

Figure 6 shows the mean position error of the typhoon center predicted by TL959L60 GSM, TL319L40 GSM and TYM. The error of TL959L60 GSM is slightly larger than that of TL319L40 GSM. However, the number of cases is so small that the difference is not statistically meaningful. TYM performed the worst of the three models. Using early analysis to make the initial fields and lateral boundary conditions of TYM is not essential because the operational TYM had been outperformed in track forecasts by the operational TL319L40 GSM starting from early analysis (not shown).

The root mean square error (RMSE) and the mean error (ME) of the typhoon central pressure forecasts are shown in Figure 7. The RMSE of TL959L60 GSM is nearly the same as that of TYM, and the difference is insignificant considering the small number of cases. The ME values for TL959L60 GSM and TYM gradually decrease from nearly +12 hPa at the initial time. After the middle forecast hours, the negative ME increases to about -3 hPa in TL959L60 GSM and to about -8 hPa in TYM for 84-hour forecasts. The RMSE of TL319L40 GSM is larger than that of TL959L60 GSM and TYM due to its poor representation of typhoon intensity as shown by the large positive ME.

4. Summary and conclusions

JMA upgraded the resolution of GSM from TL319L40 to TL959L60 in November 2007, when the TYM retired from operational use. Since then, TC track and intensity forecasts have been supported by GSM only, which provides NWP products four times a day for all TCs worldwide. Detailed representation of synoptic and sub-synoptic features such as TC structures in GSM has been

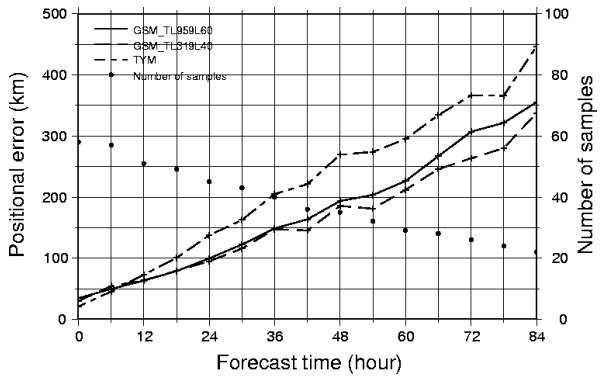

Figure 6 Mean position error of the typhoon center predicted by TL959L60 GSM (solid line), TL319L40 GSM (broken line) and TYM (dot-dash line). The numbers of samples are indicated by the dots.

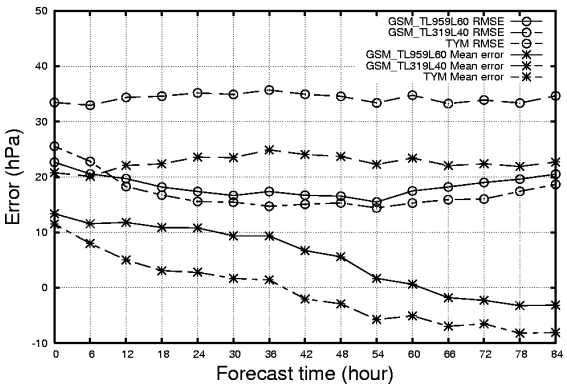

Figure 7 RMSE (circles) and mean error (asterisks) of typhoon central pressure predicted by TL959L60 GSM (solid line), TL319L40 GSM (broken line) and TYM (dot-dash line).

enabled by the enhancement of resolution. In August 2008, a reduced Gaussian grid was implemented in GSM as a new dynamical core that eliminates redundancy by cutting grid points at high latitudes, thus saving on computational resources. Verification of TC forecasts showed that TL959L60 GSM performed better than or as well as TL319L40 GSM and TYM considering the small number of TC cases in the experimental period. TL959L60 GSM also simulated the distribution and intensity of precipitation better than the other two models, including orographic precipitation and heavy rainfall near the center of the TC.

To further improve the accuracy of GSM, JMA plans to upgrade the physical package of the model. The treatment of condensed water in cumulus updraft will be refined to include the detrainment of rainwater and cloud water between the cloud base and the cloud top. The convective downdraft scheme will also be revised to calculate the downdraft ensemble corresponding to the updraft ensemble. Plans are also under way for a mixed-layer ocean model to be coupled with GSM to improve TC intensity forecast. Development of a revised 4D-Var data assimilation system has been started to incorporate the two-time-level semi-Lagrangian advection scheme and the reduced Gaussian grid used in GSM.

Appendix. NWP products

Facsimile charts from NWP are transmitted to local meteorological observatories and weather stations via domestic communication lines, and to National Meteorological Services via GTS. Another set of facsimile charts for users on ships is disseminated by JMH. The contents of the charts are listed in Table A1. The GPV products of NWP are transmitted to JMA's meteorological observatories, weather stations, the Meteorological Satellite Center and the Meteorological Research Institute as well as to the Japan Meteorological Business Support Center (JMBSC). General users in Japan, including private weather service corporations and news media, can obtain GPV products from JMBSC. Specific GPV products are customized and transmitted to relevant governmental organizations. GPV products of GSM are provided to National Meteorological Services through GTS. Two kinds of Internet data service have also been set up to facilitate the use of GPV. One is a data service based on the WMO DDB project (http://ddb.kishou.go.jp/), and the other is based on the RSMC DSS. The GPV products of GSM are listed in Table A2.

References

Iwamura, K. and H. Kitagawa, 2008: An upgrade of the JMA Operational Global NWP Model. CAS/JSC WGNE Res. Act. in Atmos. and Ocea. Modelling, **38**, 6.3-6.4.

Miyamoto, K., 2006: Introduction of the Reduced Gaussian Grid into the Operational Global NWP Model at JMA. CAS/JSC WGNE Res. Act. in Atmos. and Ocea. Modelling, **36**, 6.9-6.10.

Nakagawa, M., 2008: Improvement of the Cumulus Parameterization Scheme of the Operational Global NWP Model at JMA. CAS/JSC WGNE Res. Act. in Atmos. and Ocea. Modelling, **38**, 4.9-4.10.

Table A1 List of facsimile charts transmitted through GTS and JMH. Symbols for contents: Z: geopotential height, ζ: vorticity, T: temperature, D: dewpoint depression, ω: vertical velocity, W: wind speed by isotach, A: wind arrows, P: sea-level pressure, R: rainfall.

Area	Contents and level	Forecast hours	Initial time	Availability
Far East	500 hPa (Z, ζ)	Analysis	00/12 UTC	GTS
		24, 36	00/12 UTC	GTS/JMH
	500 hPa (T), 700 hPa (D)	24, 36	00/12 UTC	GTS/JMH
	700 hPa (ω), 850 hPa (T, A)	Analysis	00/12 UTC	GTS
		24, 36	00/12 UTC	GTS/JMH
	Surface (P, R, A)	24, 36	00/12 UTC	GTS/JMH
East Asia	300 hPa (Z, T, W, A)	Analysis	00 UTC	GTS
	500 hPa (Z, T, A)	Analysis	00/12 UTC	GTS/JMH
	500 hPa (Z, ζ)	48, 72	00/12 UTC	GTS
	700 hPa (Z, T, D, A)	Analysis	00/12 UTC	GTS
	700 hPa (ω), 850 hPa (T, A)	48, 72	12 UTC	GTS
	850 hPa (Z, T, D, A)	Analysis	00/12 UTC	GTS/JMH
	Surface (P, R)	24	00/12 UTC	GTS
		48, 72	00/12 UTC	JMH
		96, 120	12 UTC	JMH
Asia	500 hPa (Z, ζ)	96, 120, 144, 168, 192	12 UTC	GTS
	850 hPa (T), Surface (P)			
Asia Pacific	200 hPa (Z, T, W), Tropopause (Z)	Analysis	00/12 UTC	GTS
	250 hPa (Z, T, W)	Analysis, 24	00/12 UTC	
	500 hPa (Z, T, W)		00/12 UTC	
Northern Hemisphere	500 hPa (Z, T)	Analysis	12 UTC	GTS
North West Pacific	200 hPa (streamline)	Analysis, 24, 48	00/12 UTC	GTS
	850 hPa (streamline)		00/12 UTC	
	500 hPa (Z, Z anomaly to climatology)			

Xie, S. C. and M. H. Zhang, 2000: Impact of the convective triggering function on single-column model simulations. J. Geophys. Res., **105**, 14983-14996.

Yamaguchi, M. and T. Komori, 2009: Outline of the Typhoon Ensemble Prediction System at the Japan Meteorological Agency. RSMC Tokyo-Typhoon Center Technical Review, **11**, 14-24.

Yoshimura, H. and T. Matsumura, 2003: A Semi-Lagrangian Scheme Conservative in the Vertical Direction. CAS/JSC WGNE Res. Act. in Atmos. and Ocea. Modelling, **33**, 3.19-3.20.

Table A2　List of GPV products (GRIB) transmitted through GTS, DDB and RSMC DSS.

Symbols for contents: Z: geopotential height, U: eastward wind, V: northward wind, T: temperature, D: dewpoint depression, H: relative humidity, ω: vertical velocity, ζ: vorticity, ψ: stream function, χ: velocity potential, P: sea-level pressure, R: rainfall.　Symbols °*¶§‡† indicate limitations on forecast hours or initial time as shown in the table below.

Destination	GTS	GTS	DDB	DDB
Area and resolution	20°S–60°N, 60°E–160°W 1.25°×1.25°	Whole globe, 2.5°×2.5°	20°S–60°N, 60°E–160°W 1.25°×1.25°	Whole globe, 2.5°×2.5°
Levels and elements	10 hPa: Z,U,V,T 20 hPa: Z,U,V,T 30 hPa: Z,U,V,T 50 hPa: Z,U,V,T 70 hPa: Z,U,V,T 100 hPa: Z,U,V,T 150 hPa: Z,U,V,T 200 hPa: Z§,U§,V§,T§,ψ,χ 250 hPa: Z,U,V,T 300 hPa: Z,U,V,T,D 400 hPa: Z,U,V,T,D 500 hPa: Z§,U§,V§,T§,D§,ζ 700 hPa: Z§,U§,V§,T§,D§,ω 850 hPa: Z§,U§,V§,T§,D§,ω ,ψ,χ 925 hPa: Z,U,V,T,D,ω 1000 hPa: Z,U,V,T,D Surface: P¶,U¶,V¶,T¶,D¶,R¶	10 hPa: Z*,U*,V*,T* 20 hPa: Z*,U*,V*,T* 30 hPa: Z°,U°,V°,T° 50 hPa: Z°,U°,V°,T° 70 hPa: Z°,U°,V°,T° 100 hPa: Z°,U°,V°,T° 150 hPa: Z*,U*,V*,T* 200 hPa: Z,U,V,T 250 hPa: Z°,U°,V°,T° 300 hPa: Z,U,V,T,D*‡ 400 hPa: Z*,U*,V*,T*,D*‡ 500 hPa: Z,U,V,T,D*‡ 700 hPa: Z,U,V,T,D 850 hPa: Z,U,V,T,D 1000 hPa: Z,U*,V*,T*,D*‡ Surface: P,U,V,T,D*‡,R†	100 hPa: Z,U,V,T 150 hPa: Z,U,V,T 200 hPa: Z,U,V,T,ψ,χ 250 hPa: Z,U,V,T 300 hPa: Z,U,V,T,D 400 hPa: Z,U,V,T,D 500 hPa: Z,U,V,T,D,ζ 700 hPa: Z,U,V,T,D,ω 850 hPa: Z,U,V,T,D,ω, ψ,χ 925 hPa: Z,U,V,T,D,ω 1000 hPa: Z,U,V,T,D Surface: P,U,V,T,D,R	100 hPa: Z,U,V,T 200 hPa: Z,U,V,T 250 hPa: Z,U,V,T 300 hPa: Z,U,V,T 500 hPa: Z,U,V,T 700 hPa: Z,U,V,T,D 850 hPa: Z,U,V,T,D Surface: P,U,V,T,D,R†
Forecast hours	0–84 every 6 hours § additional 96–192 every 24 hours for 12 UTC ¶ 0–192 every 6 hours	0–72 every 24 hours and 96–192 every 24 hours for 12 UTC ° 0–120 for 12 UTC † Except analysis * Analysis only	0–72 every 6 hours	0–72 every 24 hours † Except analysis
Initial times	00 UTC, 06 UTC, 18 UTC and 12 UTC	00 UTC and 12 UTC ‡ 00 UTC only	00 UTC and 12 UTC	12 UTC

Table A2 (cont.)

Destination	RSMC DSS	RSMC DSS	RSMC DSS	RSMC DSS
Area and resolution	Whole globe, 1.25°×1.25°	20°S–60°N, 60°E–160°W 1.25°×1.25°	Whole globe, 2.5°×2.5°	20°S–60°N, 80°S–160°W 2.5°×2.5°
Levels and elements	10 hPa: Z,U,V,T 20 hPa: Z,U,V,T 30 hPa: Z,U,V,T 50 hPa: Z,U,V,T 70 hPa: Z,U,V,T 100 hPa: Z,U,V,T 150 hPa: Z,U,V,T 200 hPa: Z,U,V,T,ψ,χ 250 hPa: Z,U,V,T 300 hPa: Z,U,V,T,H,ω 400 hPa: Z,U,V,T,H,ω 500 hPa: Z,U,V,T,H,ω,ζ 600 hPa: Z,U,V,T,H,ω 700 hPa: Z,U,V,T,H,ω 850 hPa: Z,U,V,T,H,ω,ψ,χ 925 hPa: Z,U,V,T,H,ω 1000 hPa: Z,U,V,T,H,ω Surface: P,U,V,T,H,R†	10 hPa: Z,U,V,T 20 hPa: Z,U,V,T 30 hPa: Z,U,V,T 50 hPa: Z,U,V,T 70 hPa: Z,U,V,T 100 hPa: Z,U,V,T 150 hPa: Z,U,V,T 200 hPa: Z§,U§,V§,T§,ψ,χ 250 hPa: Z,U,V,T 300 hPa: Z,U,V,T,D 400 hPa: Z,U,V,T,D 500 hPa: Z§,U§,V§,T§,D§,ζ 700 hPa: Z§,U§,V§,T§,D§,ω 850 hPa: Z§,U§,V§,T§,D§,ω, ψ,χ 925 hPa: Z,U,V,T,D,ω 1000 hPa: Z,U,V,T,D Surface: P¶,U¶,V¶,T¶,D¶,R¶	10 hPa: Z*,U*,V*,T* 20 hPa: Z*,U*,V*,T* 30 hPa: Z*,U*,V*,T* 50 hPa: Z*,U*,V*,T* 70 hPa: Z*,U*,V*,T* 100 hPa: Z°,U°,V°,T° 150 hPa: Z*,U*,V*,T* 200 hPa: Z,U,V,T 250 hPa: Z°,U°,V°,T° 300 hPa: Z,U,V,T,D*‡ 400 hPa: Z*,U*,V*,T*,D*‡ 500 hPa: Z,U,V,T,D*‡ 700 hPa: Z,U,V,T,D 850 hPa: Z,U,V,T,D 1000 hPa: Z*,U*,V*,T*,D*‡ Surface: P,U,V,T,D*‡,R†	100 hPa: Z,U,V,T 150 hPa: Z,U,V,T 200 hPa: Z,U,V,T 250 hPa: Z,U,V,T 300 hPa: Z,U,V,T 500 hPa: Z,U,V,T,D,ζ 700 hPa: Z,U,V,T,D,ω 850 hPa: Z,U,V,T,D,ω Surface: P,U,V,T,D,R
Forecast hours	0–84 every 6 hours and 96–192 every 12 hours † Except analysis	0–84 every 6 hours § additional 96–192 every 24 hours for 12 UTC ¶ 0–192 every 6 hours	0–72 every 24 hours and 96–192 every 24 hours for 12 UTC ° 0–120 for 12 UTC † Except analysis * Analysis only	0–36 every 6 hours, 48, 60, and 72 hours
Initial times	00 UTC, 06 UTC, 18 UTC and 12 UTC	00 UTC, 06 UTC, 18 UTC and 12 UTC	00 UTC and 12 UTC ‡ 00UTC only	00 UTC and 12 UTC

Outline of the Typhoon Ensemble Prediction System at the Japan Meteorological Agency

Munehiko Yamaguchi
Numerical Prediction Division, Japan Meteorological Agency
(Present affiliation: Rosenstiel School of Marine and Atmospheric Science, University of Miami)

Takuya Komori
Numerical Prediction Division, Japan Meteorological Agency

Abstract

The Japan Meteorological Agency (JMA) began operation of a new Ensemble Prediction System (EPS) known as the Typhoon EPS (TEPS) in February 2008. TEPS has been designed to improve track forecast targeting for tropical cyclones (TCs) in the Regional Specialized Meteorological Center (RSMC) Tokyo - Typhoon Center's area of responsibility within the framework of WMO. It runs up to four times a day with a forecast range of 132 hours. The ensemble size is chosen as 11, and a singular vector method is employed to make initial perturbations.

The results of TEPS verification during a quasi-operational period from May to December of 2007 showed that ensemble mean track forecasts have a statistically better performance than deterministic forecasts under non-perturbed runs; the error reduction is 40 km in five-day forecasts. Moreover, there is a strong spread-skill relationship between the position errors of the ensemble mean and the ensemble spreads of tracks, indicating that TEPS would be useful in representing the confidence level of TC track forecasts.

1. Introduction

In 1997, the Japan Meteorological Agency (JMA) began providing three-day track forecasts of tropical cyclones (TCs) in the western North Pacific, including the South China Sea, based on numerical weather prediction (NWP) (JMA, 1997). Since then, we have seen a significant improvement in track forecasting due to the remarkable progress of the NWP system. According to verification of the global NWP system at JMA, the three-year running mean of position errors in five-day forecasts in 2007 (451 km – the average of 2005, 2006 and 2007) is smaller than that of three-day forecasts in 1997 (472 km – the average of 1995, 1996 and 1997). This indicates that we have succeeded in gaining a two-day lead time in deterministic TC track forecasts over the past decade.

While the accuracy of TC track forecasts has drastically improved, it is also true that forecast uncertainty is inevitable due to the chaotic behavior of the atmosphere and imperfections in the NWP system. Accordingly, a certain amount of forecast error should be added to each track forecast. (Puri et al., 2001; WMO, 2008a). JMA uses probability circles to express uncertainties in positional forecasting; a TC is expected to move into the circle with a probability of 70 % at a certain forecast time. The radius is determined statistically as a function of the forecast time, the direction of movement and the velocity of movement in consideration of recent years' results of verification for TC track forecasts at JMA.

Under these conditions of deterministic and probabilistic forecasting at JMA, TEPS is expected to further improve the accuracy of track forecasts using the ensemble mean and to enable proper estimation of the uncertainty of each forecast event using the ensemble spread, making it possible to optimize the radius of the probability circle flow-dependently. In order to assess the performance of TEPS, we conducted quasi-operational runs from May to December of 2007.

This report describes the results of verification during this period as well as the specifications of the system. Section 2 describes the specifications of TEPS, the NWP system and the method of making initial perturbations. Section 3 describes the performance of TEPS, the position errors of the ensemble mean and the spread-skill relationship between the position errors of the ensemble mean and the ensemble spreads of tracks. A summary and conclusions are given in Section 4.

2. Specifications

2.1 General specifications

TEPS is operated for TCs analyzed by the Regional Specialized Meteorological Center (RSMC) Tokyo - Typhoon Center. It runs up to four times a day starting at 0000, 0600, 1200 and 1800 UTC with a forecast range of 132 hours when one of the following conditions is satisfied:

1. a TC of tropical storm (TS) intensity (the maximum sustained wind speed of 34 knots to 47 knots near the centre) or higher exists in the RSMC Tokyo - Typhoon Center's area of responsibility (0 – 60N, 100 – 180E);
2. a TC is expected to reach TS intensity or higher in the area within 24 hours;
3. a TC of TS intensity or higher is expected to move into the area within 24 hours.

The NWP model for TEPS is a global model with a resolution of TL319L60, which is a lower-resolution version of the JMA Global Spectral Model (JMA/GSM) at TL959L60 (Iwamura and Kitagawa, 2008; Nakagawa, 2009). Global analysis for JMA/GSM at TL959L60, which is based on a four-dimensional variational data assimilation system (4DVAR) (Kadowaki, 2005; JMA, 2007), is interpolated to TL319L60 and used as the initial condition of TEPS. The ensemble size is set at 11 with one non-perturbed run and ten perturbed runs, where the perturbations are generated using the singular vector (SV) method (Buizza, 1994; Molteni et al., 1996; Puri et al., 2001) (see Section 2-2 for details).

2.2 Initial perturbations

TEPS adopts an SV method to generate initial perturbations. If a perturbation grows linearly, an SV with a large singular value represents a fast-growing perturbation (Lorenz, 1965). In addition, using an SV method enables the computation of perturbations that have a large influence on an arbitrarily chosen domain, which can be associated with the development or movement of TCs when the domain is targeted to the TC's surroundings.

The tangent-linear and adjoint models used for SV computation come from 4DVAR, which has been in operation since February 2005. While their resolutions were T159L60 for 4DVAR as of September 2008, TEPS uses the lower-resolution version T63L40. The models consist of full dynamical core and physical processes including vertical diffusion, gravity wave drag, large-scale condensation, long-wave radiation and deep cumulus convection. SVs based on the tangent-linear and adjoint models including the full physical processes (the simplified physical processes without moist processes) are called moist (dry) SVs. TEPS calculates dry SV targeting for the mid-latitude area in the RSMC Tokyo - Typhoon Center's area of responsibility, aiming to identify the dynamically most unstable modes of the atmosphere, such as the baroclinic mode (Buizza and Palmer, 1995). It also calculates moist SV targeting for TC surroundings where moist processes are critical (Barkmeijer et al., 2001).

JMA's computing system allows TEPS to target up to three TCs at a time. If more than three TCs are present, three of them are selected in the order of concern of the RSMC Tokyo - Typhoon Center. The targeted area of dry SV calculations is fixed as 20 – 60N, 100 – 180E, and that of moist SV calculations covers a rectangle of 10 degrees in latitude and 20 degrees in longitude with its center at the forecasted TC's central position at a forecast time of 24 hours. The optimization time interval for SV calculations is 24 hours for both dry and moist SVs. As shown in the following equation (1), the norm to evaluate the growth rate of dry and moist SVs is based on a total energy norm that includes a specific humidity term (Barkmeijer et al., 2001):

$$
\begin{aligned}
(x, \mathbf{E}x) \;=\; & \frac{1}{2}\int_0^1 \int_S (\nabla\Delta^{-1}\zeta_x \cdot \nabla\Delta^{-1}\zeta_x + \nabla\Delta^{-1}D_x \cdot \nabla\Delta^{-1}D_x \\
& + g(\Gamma_d - \Gamma)^{-1}\frac{T_x T_x}{T_r} \\
& + w_q \frac{L_c^2}{c_p T_r} q_x q_x) dS \left(\frac{\partial p}{\partial \eta}\right) d\eta \\
& + \frac{1}{2}\int_S \frac{R_d T_r}{P_r} P_x P_x dS
\end{aligned}
\qquad (1)
$$

where ζ_x, D_x, T_x, q_x and P_x are the vorticity, divergence, temperature, specific humidity and surface pressure components of vector x, and **E** represents a norm operator. Note that the temperature lapse rate Γ is taken into consideration as an available potential energy term (Lorenz, 1955). c_p is the specific heat of dry air at a constant pressure, L_C is the latent heat of condensation, and R_d is the gas constant for dry air. T_r = 300 K is a reference temperature, Pr = 800 hPa is a reference pressure, and

w_q is a constant (w_q = 1 in TEPS). The representative value of $2/3\Gamma_d$ is used for Γ. In Eq. (1), the vertical integration of the kinetic energy term and the available potential energy term is limited to 100 hPa (the 26th model level), and the specific humidity term can be up to 500 hPa (the 15th model level). Otherwise, as is the case with the study by Barkmeijer et al. (2001), SVs have a shallow vertical structure in the upper troposphere or have a large specific humidity contribution in the upper troposphere where the amount of specific humidity is relatively small. Since such SVs have little influence on TC track forecasts, we set a limit on the vertical integration in Eq. (1).

Finally, initial perturbations are generated by linearly combining SVs. Each SV calculation can produce up to ten SVs depending on the operationally allocated calculation time period, which means that up to 40 SVs can be obtained (i.e., 10 dry SVs and 30 moist SVs) for one forecast event. Before determining the binding coefficients, SVs with structures similar those of others are eliminated. When the value of the inner product of any two SVs is 0.5 or more, one of them is eliminated from the group of SV candidates used to make initial perturbations. After this process, the binding coefficients are determined based on a variance minimum rotation, which makes the spatial distributions of the perturbations widely spread. If no SV is eliminated, we have the same number of independent initial perturbations as the number of SVs computed. For the ten perturbed runs, we select five perturbations randomly from the initial perturbations, and positively and negatively add them to the analysis field. The amplitude of the perturbations is adjusted so that the maximum zonal or meridional wind speed equals 6.0 m/s.

Table 1 gives a summary of the specifications. It should be noted that JMA also operates the One-Week Ensemble Prediction System (WMO 2008b), which has specifications similar to those of TEPS but is designed to improve medium-range forecasts. For reference, we add the specifications of the EPS shown in Table 1.

Table 1 Specifications of the Ensemble Prediction Systems at JMA

		Typhoon Ensemble Prediction System (TEPS)		One-Week Ensemble Prediction System (WEPS)	
Forecast domain		Global			
Truncation wave number		Spectral triangular truncation at 319 wave numbers with linear Gaussian grid (TL319)			
Horizontal grid, grid spacing		640 x 320, 0.5625 deg. (– 60 km)			
Vertical resolution		60 unevenly spaced hybrid levels (from surface to 0.1 hPa)			
Forecast range		132 hours		216 hours	
Initial time		00, 06, 12, 18 UTC		12 UTC	
Ensemble size		11 members (10 perturbed forecasts and 1 control forecast)		51 members (50 perturbed forecasts and 1 control forecast)	
Perturbation	Perturbation generator	Singular Vector (SV) method			
	Inner model resolution	Spectral triangular truncation at 63 wave numbers (T63), 40 unevenly spaced hybrid levels (from surface to 0.4 hPa)			
	Norm	Moist total energy			
	Perturbed area	Western North Pacific (20 – 60N, 100 – 180E)	3 Typhoons (20 deg. x 10 deg. in the vicinity of each typhoon)	Northern Hemisphere (30 – 90N)	Tropics (20S – 30N)
	Physical process	*Simplified physics	**Full physics	*Simplified physics	**Full physics
	Optimization time interval	24 hours		48 hours	24 hours
	Evolved SV	Not used		Used	

*Simplified physics: initialization, horizontal diffusion, surface turbulent diffusion and vertical turbulent diffusion

**Full physics: the elements of simplified physics plus gravity wave drag, long wave radiation, large-scale condensation and cumulus convection

3. Performance

3.1 Case studies

Figure 1 shows examples of forecasts using TEPS. The upper figures are for typhoon Maria in 2006, initiated at 12 UTC on Aug. 6th, 2006, and the lower figures are for typhoon Chaba in 2004, initiated at 12 UTC on Aug. 28th, 2004. The panels on the left show track forecasts by JMA/GSM (the solid lines) with a best track (the dashed line), while those on the right show all tracks obtained using TEPS. In the case of Maria, there is a large ensemble spread; some of the ensemble members support the same scenario as JMA/GSM, indicating that Maria is heading for western Japan, while others recurve and head toward eastern Japan. In reality, as the best track shows, Maria recurved

and skirted the southern coast of the Kanto region to the east of Japan. It is noteworthy that TEPS captured the possibility of the best track. From the perspective of disaster prevention or mitigation, it is very important to ascertain all possible scenarios in advance and take measures as needed. TEPS is expected to enable the capture of such potential track spreads. In contrast to the case with Maria, Chaba shows quite a small ensemble spread, meaning that the confidence of the forecast is relatively high. In fact, the deterministic forecast by JMA/GSM was almost perfect. As in these two cases, we can expect TEPS to provide track forecast information with high confidence referring to ensemble spreads that could vary by TC and the initial time of forecasting.

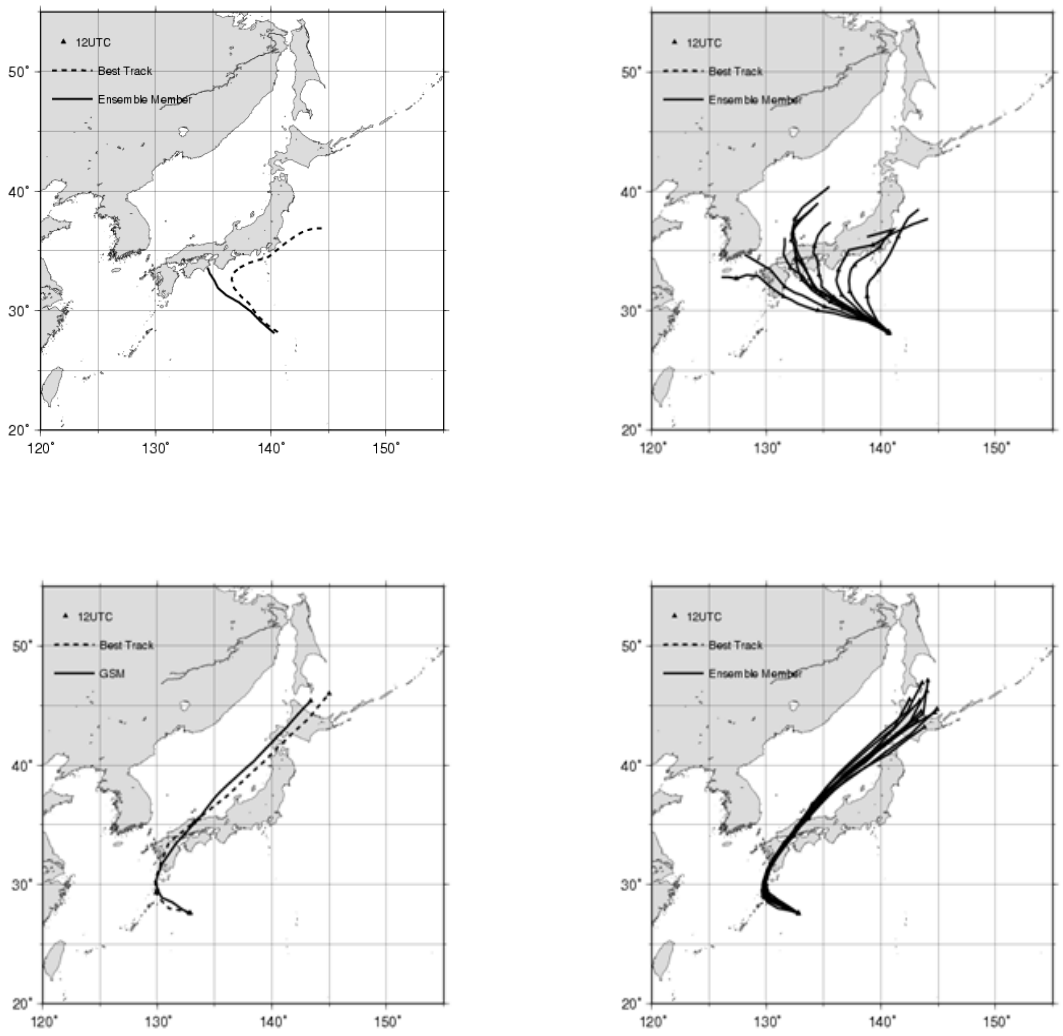

Figure 1. Example forecasts of TEPS. The upper figures are for typhoon Maria in 2006, initiated at 12 UTC on Aug. 6th, 2006. The lower figures are for typhoon Chaba in 2004, initiated at 12 UTC on Aug. 28th, 2004. The figures on the left show the track forecast by JMA/GSM (the solid line) with the best track (the dashed line), and those on the right show all tracks forecast using TEPS.

3.2 Quasi-operational application

To statistically evaluate the performance of TEPS, we conducted quasi-operational runs of TEPS from May to December of 2007. We verified the ensemble mean tracks and the spread-skill relationship between the position errors of the ensemble mean and the ensemble spreads of tracks. The specifications of quasi-operational TEPS are different from those of operational TEPS in several respects. For example, the fields analyzed by TEPS before November 21st, 2007 (when high resolution JMA/GSM with TL959L60 became operational) come from those of the lower-resolution JMA/GSM with TL319L40. However, we confirmed through one-month period experimentation that these differences in specifications have little influence on the performance.

3.2.1 Ensemble mean track forecast

Figure 2 shows the position errors of the ensemble mean track, which is made by averaging all forecasted TC tracks. The verifications are based on the best track data produced by the RSMC Tokyo - Typhoon Center. Both Figures 2a and 2b are the results of verifying TCs of tropical storm intensity or higher, but Figure 2b includes the extratropical-transition stages of TC verification. The X-axis represents the forecast time up to five days. The Y-axis on the left gives the position errors (in km) of control runs, or non-perturbed runs (the thin line), and the ensemble mean (the thick line). The dots correspond to the Y-axis on the right, which represents the number of verification samples. As both Figures 2a and 2b show, the position errors of the ensemble mean are smaller than those of the control runs in four- and five-day forecasts, although their performance as control runs up to the three-day forecast point is almost identical. The error reduction in five-day forecasts is 40 km (as shown in Figure 2a), which is equivalent to a gain of about half a day of lead time, given that the position error difference between four-day and five-day forecasts by JMA's global forecasting NWP system was about 100 km in 2007 (see Figure 3).

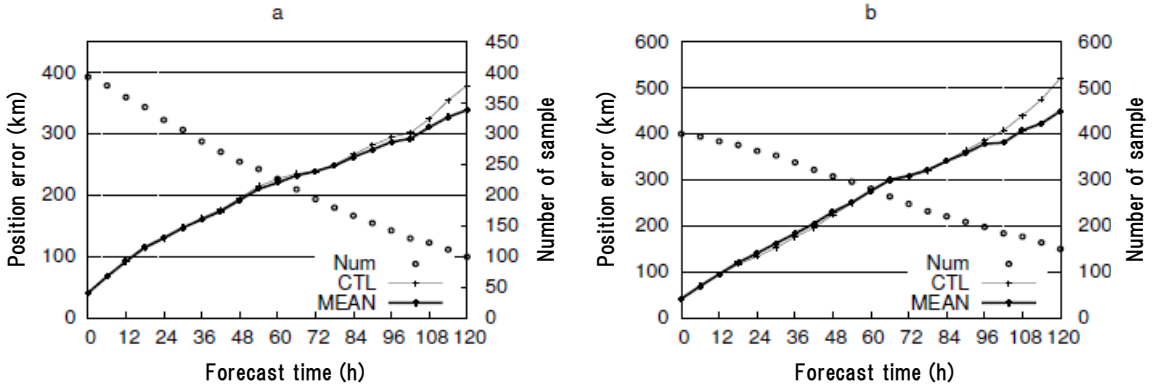

Figure 2. Position errors (in km) of the ensemble mean (the thick lines) as a function of the forecast time up to 120 hours, compared with those of control runs (the thin lines). The dotted lines correspond to the Y-axis on the right, which represents the number of verification samples. Both a and b are the results of verifying TCs of tropical storm intensity or higher, but b includes the extratropical-transition stages of the TCs verified. The verification period was the quasi-operation period of TEPS from May to December, 2007.

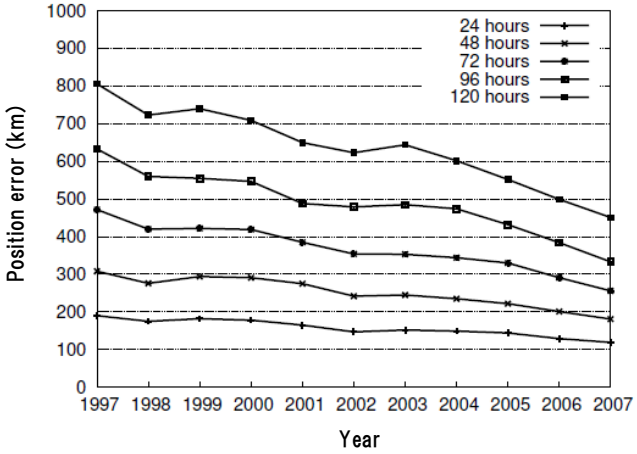

Figure 3. Time series of the three-year running mean of position errors by JMA's global forecasting NWP system from 1997 to 2007 (e.g., the verification value for 2007 is the average of those for 2005, 2006 and 2007). Each line represents the errors of 24-, 48-, 72-, 96- and 120-hour forecasts from the bottom up.

3.2.2 Spread-skill relationship

Figure 4 shows the spread-skill relationship of five-day track forecasts. The TCs verified are exactly the same as those in Figure 2b, and each dot gives the verification result of each forecast event. As Figure 4 shows, there is a strong spread-skill relationship; when ensemble spreads are relatively small, the position errors of the corresponding forecast events are also small. More importantly, there are no cases with large position errors, which occur when ensemble spreads are relatively large. While Figure 4's verification is limited to a forecast time of five days, a strong spread-skill relationship can be seen in verifications for other forecast times.

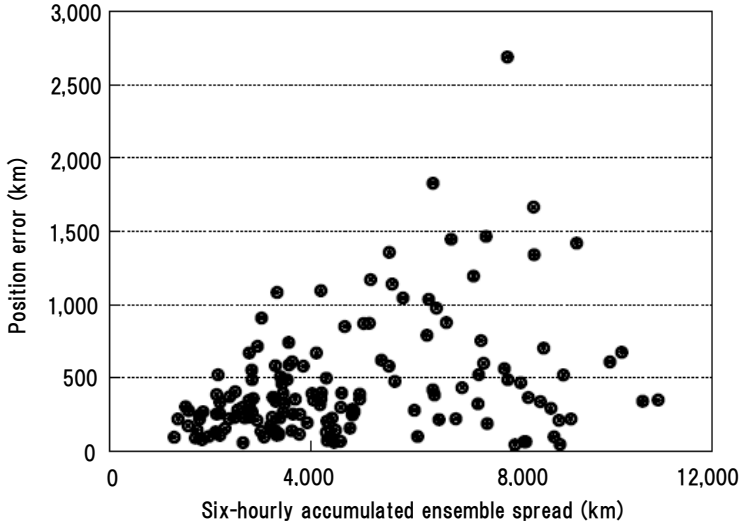

Figure 4. Spread-skill relationship of five-day track forecasts. The X-axis represents ensemble spreads (km) accumulated every six hours from the initial time to the five-day stage. The Y-axis represents the position errors (km) of the ensemble mean for the corresponding forecast events. The total number of cases is 149, which is the same as that of the five-day forecasts in Figure 2b.

Based on this relationship, we classify the confidence level of TC track forecasts (i.e., ensemble mean track forecasts) at each forecast time for each forecast event. A confidence index (A, B or C, representing the categories of the highest, middle-level and lowest confidence, respectively) is allocated, and the frequency of each category is set to 40%, 40% and 20 % respectively. Figure 5 shows that the average position errors in category A are quite small in comparison to those of all track forecasts shown in Figure 2b. As an example, the position errors of three-day forecasts are about 300 km on average, but become less than 200 km if the samples are limited to cases with small ensemble spreads. Conversely, the average position errors in category C are larger than the those of all forecasts.

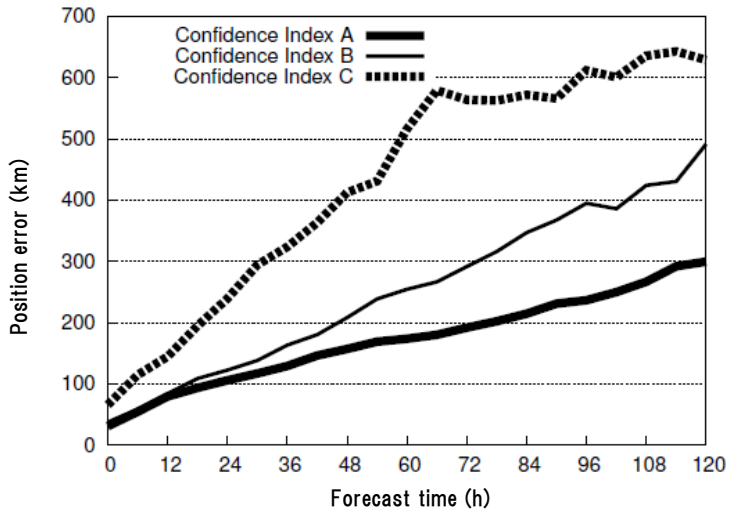

Figure 5. Verification results of confidence indices on TC track forecasts. Referring to the amount of ensemble spread, a confidence index (A, B or C) is given to ensemble mean track forecasts at each forecast time for each forecast event (A represents the highest level of confidence). The thick line shows the position errors of the ensemble mean for all A cases as a function of the forecast time. The thin and dashed lines represent the B and C cases, respectively.

The reason why the categories are set as 40%, 40% and 20% (rather than 33%, 33% and 33%) is to clearly split the position errors into three lines as in Figure 5. Figure 6 shows the position error of each three-day forecast by JMA's global NWP system in 2007 with the errors sorted in ascending order. As the figure shows, the frequency distribution of the errors is not uniform, and the rate of cases with a relatively large position error is about 10 to 20% of the total number of events. We therefore set the rate of category C to be smaller than those of categories A and B.

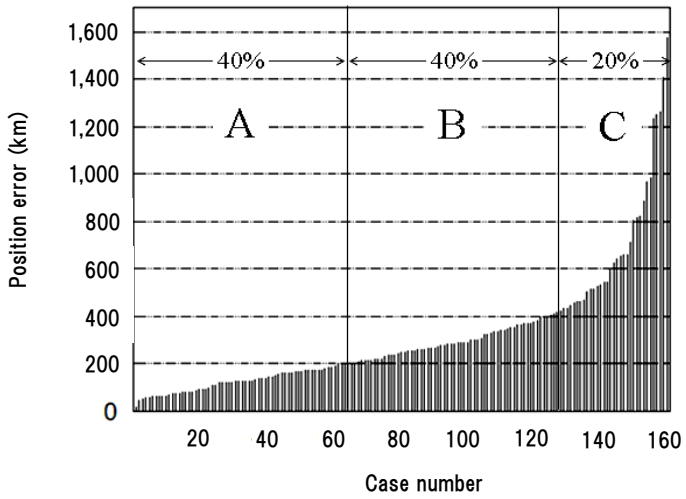

Figure 6. Position error (km) of each three-day track forecast initiated at 00 UTC by JMA's global forecasting NWP system in 2007. The errors are sorted in ascending order, and the total number of cases is 163.

4. Summary

JMA began operation of the new Typhoon EPS in February 2008 with the aim of improving TC track forecasts. TEPS runs up to four times a day with a forecast range of 132 hours targeting TCs in the western North Pacific, including the South China Sea. It is composed of eleven forecast members derived from the TL319L60 global model. The method of making initial perturbations is based on the SV method.

In order to assess the performance of TEPS, we conducted quasi-operational forecasts of the system from May to December of 2007. Verification of these quasi-operational runs showed that two benefits can be expected from TEPS. First, the position errors of deterministic track forecasts will be reduced. Using the ensemble mean obtained a 40-km reduction in five-day track forecasts on average, corresponding to a gain of about half a day of lead time. Second, information on track forecasts' level of confidence can also be obtained. Referring to the ensemble spreads of tracks has enabled the extraction of uncertainty information on track forecasts.

Remaining issues include the question of how to leverage the benefits of TEPS in operational forecasting. In particular, conveying uncertainty information to public users is challenging, and this point must be kept in mind during the development of related applications.

References

Barkmeijer, J., R. Buizza, T. N. Palmer, K. Puri, and J.-F. Mahfouf, 2001: Tropical singular vectors computed with linearized diabatic physics. *Quart. J. Roy. Meteor. Soc*., **127**, 685-708.

Buizza, R., 1994: Sensitivity of optimal unstable structures. *Quart. J. Roy. Meteor. Soc*., **120**, 429-451.

Buizza, R., and T. N. Palmer, 1995: The singular vector structure of the atmospheric global

circulation. *J. Atmos. Sci*., **52**, 1434-1456.

Iwamura, K. and H. Kitagawa, 2008: An upgrade of the JMA Operational Global NWP Model. *CAS/JSC WGNE Research Activities in Atmospheric and Oceanic Modelling*. (submitted)

Japan Meteorological Agency, 1997: Annual Report on Activities of the RSMC Tokyo - Typhoon Center, 115pp.

Japan Meteorological Agency, 2007: Outline of the operational numerical weather prediction at the Japan Meteorological Agency. Appendix to WMO Numerical Weather Prediction Progress Report. Japan Meteorological Agency, Tokyo, Japan. Available online at http://www.jma.go.jp/jma/jma-eng/jma-center/nwp/outline-nwp/index.htm

Kadowaki, T., 2005: A 4-dimensional variational assimilation system for the JMA Global Spectrum Model. *CAS/JSC WGNE Research Activities in Atmospheric and Oceanic Modelling*, **34**, 1-17.

Lorenz, E. N., 1955: Available potential energy and the maintenance of the general circulation. *Tellus*, **7**, 157-167.

Lorenz, E. N., 1965: A study of the predictability of a 28-variable atmospheric model. *Tellus*, **17**, 321-333.

Molteni, F., R. Buizza, T. N. Palmer, and T. Petroliagis, 1996: The ECMWF ensemble prediction system: Meteorology and validation. *Quart. J. Roy. Meteor. Soc*., **122**, 73-120.

Nakagawa, M., 2009: Outline of the High Resolution Global Model at the Japan Meteorological Agency. RSMC Tokyo-Typhoon Center Technical Review, **11**, 1-13.

Puri, K., J. Barkmeijer, and T. N. Palmer, 2001: Ensemble prediction of tropical cyclones using targeted diabatic singular vectors. *Quart. J. Roy. Meteor. Soc*., **127**, 709-731.

WMO, 2008a: Guidelines on Communicating Forecast Uncertainty (PWS-18), 25pp. Available online at http://www.wmo.ch/pages/prog/amp/pwsp/publicationsguidelines_en.htm

WMO, 2008b: WMO Technical Progress Report on the Global Data-Processing and Forecasting System (GDPFS) and Numerical Weather Prediction (NWP) Research. Available online at http://www.wmo.int/pages/prog/www/DPFS/ProgressReports/2007/Japan_2007.pdf

Outline of the Storm Surge Prediction Model at the Japan Meteorological Agency

Masakazu Higaki, Hironori Hayashibara, Futoshi Nozaki
Office of Marine Prediction, Japan Meteorological Agency

Abstract

Japan has suffered many storm surge disasters in the past, especially those associated with tropical cyclones (TCs). To mitigate the effects of such disasters, the Japan Meteorological Agency (JMA), which is responsible for issuing storm surge warnings, operates a numerical storm surge model to provide the basis for warnings. The model runs eight times a day and provides 33-hour predictions of storm surges and sea levels for 290 points along the Japanese coastline. When a TC enters the vicinity of Japan, the model predicts multiple scenarios of storm surges with different meteorological forcing fields to take into account the uncertainty in TC track forecasts.

1. Introduction

Storm surges, especially those associated with tropical cyclones (TCs), represent a major marine hazard, and frequently result in the loss of life and property in many parts of the world. As an example, 1970's Cyclone Bhola killed more than 200,000 people in East Pakistan (now Bangladesh), and a 1991 cyclone killed 131,000 in Bangladesh. It should be noted that most of these casualties are attributed to storm surges caused by the TCs.

As Japan is located in a region of high TC activity, it often experiences storm surge disasters caused mainly by typhoons. In 1959, Typhoon Vera (T5915) hit the central part of Japan causing more than 5,000 fatalities, most of them related to a storm surge of 3.5 m in the Ise Bay area arising from the typhoon. Even more recently, Japanese society has suffered repeated storm surge disasters. In 1999, Typhoon Bart (T9918) caused severe storm surges in the western part of Japan, killing thirteen people, and in 2004 more than 30,000 houses were flooded by storm surges induced by Typhoon Chaba (T0416) in western Japan's Seto Inland Sea.

Accurate and timely forecasts and warnings are critical in mitigating the threat to life and property posed by such storm surges. The Japan Meteorological Agency (JMA), which is responsible for issuing storm surge warnings, has operated a numerical storm surge model since 1998 to provide basic information for use in warnings. In this paper, we give an outline and describe the specifications and performance of this storm surge model. As discussed below,

the model computes only storm surges, but the issuance of storm surge warnings also requires the prediction of storm tides (i.e., the sum of the storm surge and the astronomical tide), meaning that astronomical tides must be calculated separately. However, this paper does not detail the method of astronomical tide prediction, as its focus is on the storm surge model.

2. Dynamics

Storm surges are mainly caused by the effects of wind setup due to strong onshore winds over the sea surface and the inverted barometer effect associated with pressure drops in low-pressure systems. To predict temporal and spatial sea level variations in response to such meteorological disturbances, JMA's storm surge model utilizes two-dimensional shallow water equations consisting of vertically integrated momentum equations in two horizontal directions:

$$\begin{aligned} \frac{\partial M}{\partial t} - fN &= -g(D+\zeta)\frac{\partial(\zeta-\zeta_0)}{\partial x} + \frac{\tau_{sx}}{\rho} - \frac{\tau_{bx}}{\rho} \\ \frac{\partial N}{\partial t} + fM &= -g(D+\zeta)\frac{\partial(\zeta-\zeta_0)}{\partial y} + \frac{\tau_{sy}}{\rho} - \frac{\tau_{by}}{\rho} \end{aligned} \tag{1}$$

and the continuity equation:

$$\frac{\partial \zeta}{\partial t} = -\frac{\partial M}{\partial x} - \frac{\partial N}{\partial y} \tag{2}$$

where M and N are volume fluxes in the x- and y-directions, defined as:

$$\begin{aligned} M &= \int_{-D}^{\zeta} u \mathrm{d}z \\ N &= \int_{-D}^{\zeta} v \mathrm{d}z \end{aligned} \tag{3}$$

f is the Coriolis parameter; g is the gravity acceleration; D is the water depth below mean sea level; ζ is the surface elevation; ζ_0 is the inverted barometer effect converted into an equivalent water column height; ρ is the density of water; τ_{sx} and τ_{sy} are the x- and y-components of wind stress on the sea surface; and τ_{bx} and τ_{by} are the stress values of bottom friction. For computational efficiency, non-linear advection terms are omitted.

The equations are solved by numerical integration using an explicit finite difference method.

3. Meteorological forcing

A storm surge model requires fields of surface wind and atmospheric pressure as external forcing, and these fields – especially wind – have the greatest impact on the performance of storm surge prediction. In the operation of JMA's storm surge model, two kinds of meteorological forcing field are used; one is a simple parametric model of TC structure, and the other is the prediction of the operational JMA nonhydrostatic mesoscale model (referred to below as *MSM*) (Saito *et al.*, 2006).

The parametric TC model is introduced to take into account the errors of TC track

forecasts and their influence on storm surge forecasting. Although the performance of TC forecasts has gradually improved, their mean position error remains around 100 km for 24-hour forecasts at present (JMA, 2008). This implies that there is a large spread of possible forecast values for surface wind and atmospheric pressure at a certain location, making accurate storm surge prediction difficult even for 24-hour forecasts. Figure 1 demonstrates how differences in the path of a TC change storm surge occurrence. If the typhoon veers left of the forecast track, a storm surge will occur in Osaka Bay (the western bay in the area shown in the figures) (Figure 1(b)), while a surge would occur in Ise Bay (the eastern bay in the figures) if the typhoon veers right (Figure 1(c)).

To take into account the influence of TC track uncertainty on the occurrence of storm surge, we conduct five runs of the storm surge model with five possible TC tracks. These five tracks are prescribed at the center and at four points on the probability circle within which a TC is forecast to exist with a probability of 70% (Figure 2), and are used to make meteorological fields with a parametric TC model. The simple parametric TC model used by Konishi (1995) based on Fujita's empirical formula (Fujita, 1952) is adopted. The radial pressure distribution of the simple parametric TC model is represented as follows:

$$P = P_{\infty} - \frac{P_{\infty} - P_c}{\sqrt{1 + (r / r_0)^2}} \tag{4}$$

and is related to the gradient wind as follows:

$$-\frac{v^2}{r} - fv = -\frac{1}{\rho}\frac{\partial P}{\partial r} \tag{5}$$

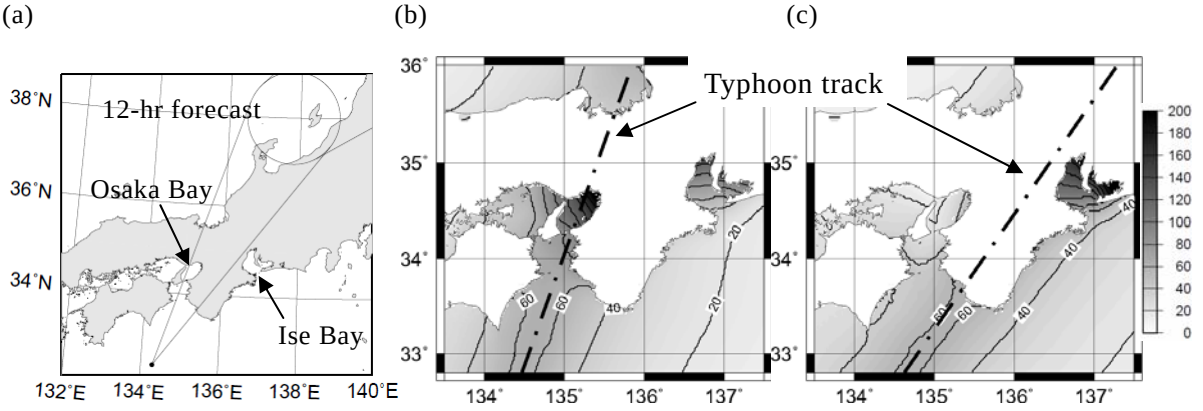

Figure 1 Maximum surge envelopes simulated with different typhoon tracks (unit: cm).
(a) The typhoon tracks used in the simulations (b) The case in which a typhoon takes the leftmost path (c) As (b), but for the rightmost path.

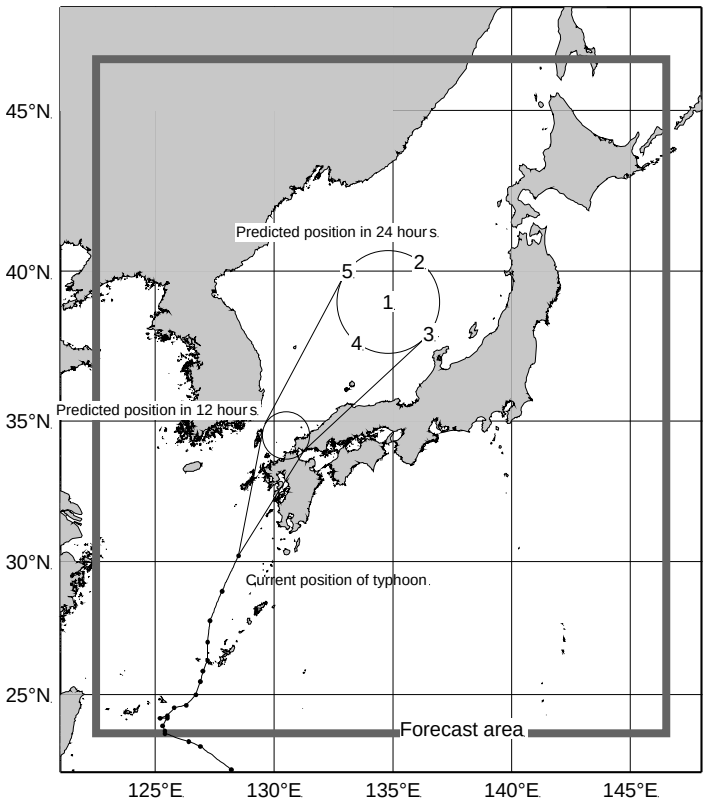

Figure 2　The model area and an example of a TC forecast track.
The circles represent areas into which the center of a TC will enter with 70% probability at each forecast time.　The numbers in and on the probability circle represent the TC tracks used in storm surge prediction. (1: center, 2: fastest, 3: rightmost, 4: slowest, 5: leftmost)

In Eqs. (4) and (5), P is the atmospheric pressure at distance r from the center of the TC, P_∞ is the atmospheric pressure at an infinitely distant point, P_c is the pressure at the TC center, r_0 is the scaling factor of the radial distribution of pressure, and v is the gradient wind speed.　The wind vectors are rotated inward 30 degrees to approximate the inflow in a TC.　For the asymmetry of the wind field in a TC, the moving velocity vector of the TC multiplied by a weight that decays exponentially with the distance from the TC center is added to the wind vector.　The resulting wind and pressure fields are applied to the storm surge model as external forcing.　These formulas diagnose wind and pressure fields at each point in time using the necessary input of forecast values as follows:

- The location (longitude and latitude) of the TC center
- The minimum pressure at the TC center
- The maximum sustained wind speed
- The radius of 50 kt wind speeds (if present)
- The radius of 1 000 hPa

These values are obtained from the tropical cyclone advisories issued by the RSMC Tokyo – Typhoon Center.

The surge model also uses wind and pressure fields predicted by MSM, which is a nonhydrostatic numerical weather prediction model with 5-km horizontal resolution. MSM runs eight times a day and provides 33-hour forecasts over the area of Japan. There are two reasons for using MSM fields in storm surge prediction. Firstly, these fields are used to predict storm surges caused by extratropical cyclones. When no TCs are present around Japan, the storm surge model predicts a single scenario using MSM prediction. Secondly, MSM generally gives more realistic wind and pressure fields than the parametric TC model when a TC is approaching the main islands of Japan. Complex meteorological processes such as extratropical transition, structural changes at the weakening stage and the effects of land topography mean that it is sometimes inappropriate to express the wind and pressure fields with the parametric TC model given by Eqs. (4) and (5). As described in Section 5, a comparative study confirmed that the use of MSM improves the accuracy of storm surge prediction, especially in short-range forecasting, because of its ability to reproduce realistic meteorological fields. JMA therefore started using MSM fields in operational storm surge prediction for TCs in September 2007.

4. Specifications and products of the model

Table 1 outlines the specifications of the storm surge model. Its horizontal resolution is one arc-minute in longitude and latitude, corresponding to an area of about 1.5 km by 1.9 km. The model area covers the whole of Japan (refer to Figure 2). The model runs eight times a day (i.e., every three hours) on JMA's high-performance computing system for numerical weather prediction, and provides 33-hour prediction of storm surges for about 290 locations along the Japanese coast.

Table 1 Specifications of the storm surge model

Area	23.5 – 46.5°N, 122.5 – 146.5°E
Grid resolution	1 arc-minute (1.5km in zonal direction, 1.9km in meridional direction)
Forecast range	33 hours
Initial time	00, 03, 06, 09, 12, 15, 18 and 21 UTC
Forecast members	6 members (in the case of tropical cyclones) 1 member (in the case of extratropical cyclones)

The model computes only storm surges, i.e., anomalies from the level of astronomical tides. However, storm tides (storm surges plus the astronomical tides) are also needed for the issuance of storm surge warnings. Astronomical tides are predicted using harmonic analysis of sea levels observed at tide stations beforehand. After the computation of the storm surge model, the level of the astronomical tide for each station is added to the predicted storm surge.

The model results are sent to local meteorological observatories that issue storm surge

warnings to their individual areas of responsibility. These warnings include information on the period and water level of possible maximum surges in the area concerned, and are used by disaster prevention organizations for the implementation of countermeasures against disasters.

Provided with appropriate sets of meteorological forcing fields and bathymetric data, this model can also predict storm surges in other areas of the world. Appendix 1 presents an example of the model's application to storm surge events in Southeast Asia.

5. Performance of the model

In this section, we describe the performance of the storm surge model with two case studies and a comparative verification of surge prediction with two different forcing fields.

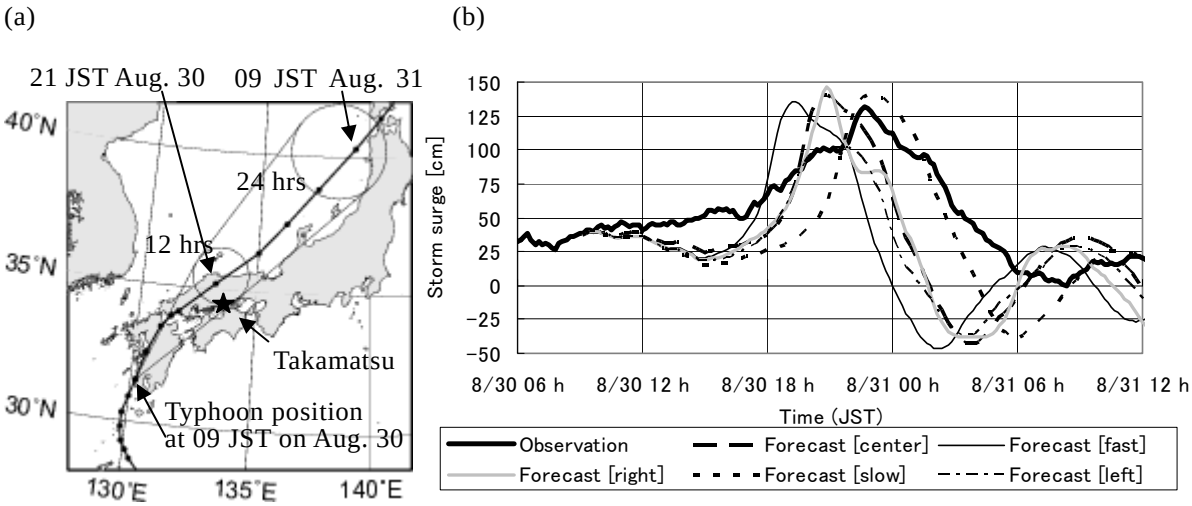

Figure 3 Track of Typhoon Chaba (T0416) and time series of a storm surge at Takamatsu.

(a) The track of the typhoon. The thick line is the analyzed track, and the dots on the line show six-hourly positions. The two circles indicate the possible areas of the typhoon's center position with 70% probability for 12-hour and 24-hour forecasts.

(b) Observed and predicted storm surges for the Takamatsu tide station.
The five thin lines depict the time series predicted for the five different typhoon tracks.

Case study 1: Typhoon Chaba (T0416)

Figure 3 shows a time series of the storm surge at the Takamatsu tide station on August 30 – 31, 2004, when Typhoon Chaba (T0416) passed the western part of Japan. This typhoon caused storm surge disasters in coastal areas in the western part of Japan, particularly those surrounding the Seto Inland Sea. Figure 3 also shows the storm surge predictions initialized at 09 JST on August 30 about 12 hours before the peak surge occurred. In this prediction, only the parametric TC model fields were used as forcing. As described above, five forecast runs were carried out for the five different possible TC tracks, and the results are denoted by the five

different lines in the figure. The heights of the forecast peak surges show close agreement with the observation results. Although the time of the predicted peak surge for the center track is slightly earlier than the observed value, this five-member ensemble predicted the probability of the time lag. Based on this model result, the Takamatsu Local Meteorological Observatory issued storm surge warnings about six hours before the sea level reached its maximum. This example can be considered to demonstrate the effectiveness of the model.

(a)

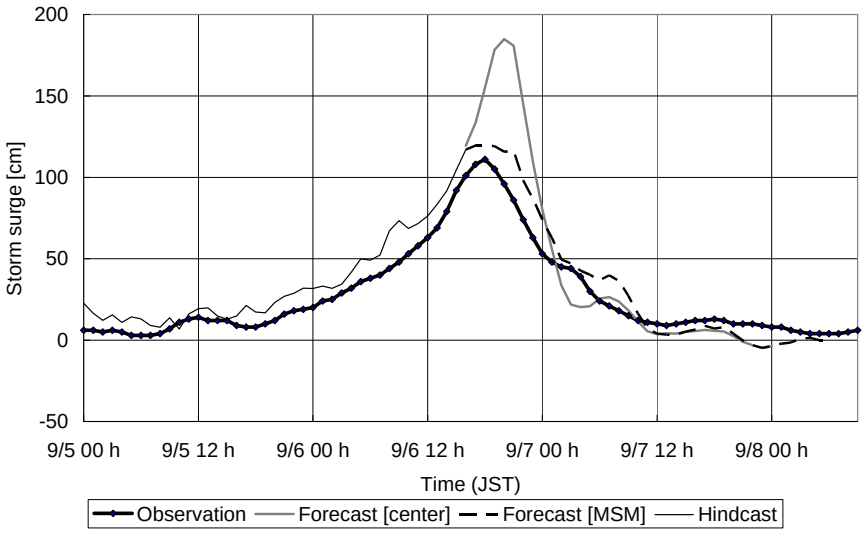

(b) (c)

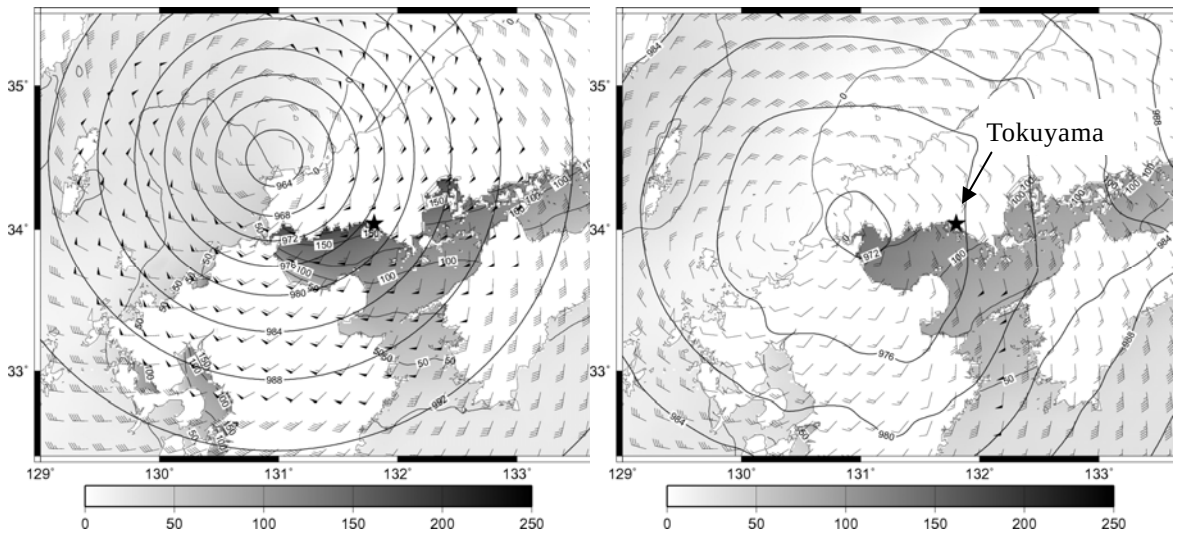

Figure 4 Storm surge of Typhoon Nabi (T0514).

(a) Time series of observed and predicted storm surge data at the Tokuyama tide station.

(b) Predicted surge distribution valid for 21 JST, 6 September 2005 (unit: cm). The surge model is driven by the fields from the parametric TC model. The wind and pressure fields are also shown.

(c) As (b), but for prediction driven by MSM.

Case study 2: Typhoon Nabi (T0514)

In the above case, the model successfully predicted the magnitude and timing of the storm surge, but in other cases it sometimes overestimated storm surges when used with the parametric TC model, as illustrated here. Figure 4 presents the storm surge caused by Typhoon Nabi (T0514). The typhoon made landfall on Kyushu in the western part of Japan after 14 JST on 6 September 2005, inducing storm surges of around a meter in adjacent coastal areas. Figure 4(a) indicates that storm surge prediction with the parametric TC model overestimated by 80 cm. To study the cause of this error, we conducted a storm surge simulation driven by the meteorological fields predicted by MSM, and compared the results with those of the parametric TC model. The time series of the surge predicted with MSM shown in Figure 4(a) agrees closely with the observation. The difference in these two surge predictions can be attributed to the difference in the wind fields used. Around the time of the peak surges, the typhoon was in the weakening stage after landfall and the wind field was affected by the complex topography of the surrounding land areas (Figure 4(c)). However, as shown in Figure 4(b), the parametric TC model gives a wind field that is symmetrical and much stronger than that of MSM. This is because it does not take into consideration factors such as the effect of land topography on the wind field, mainly due to its simple algorithm. These results suggest that the parametric TC model may overestimate wind fields in coastal areas in the weakening stage of TCs, resulting in overestimated surge prediction.

Comparative verification

To examine the performance of the storm surge model, we conducted verification of the model results by comparing them with observed storm surges. In this verification, we examined the difference in the accuracy of the predicted surges driven by two different forcing fields (the parametric TC model and MSM), since the choice of forcing field affects the accuracy of surge prediction as shown in the above case study. These two sets of surge predictions are compared with hourly storm surge values observed at about 110 tide stations along the Japanese coast for all tropical cyclones that approached or hit Japan from 2004 to 2007. For surge prediction with the parametric TC model, only the results for central TC tracks are used among the five results corresponding to the five TC tracks.

Figure 5 shows scatter diagrams of the predicted surges against the observed values. The predicted values include all those for 1-hour through 33-hour forecast times. The figures show that the surge predictions driven by the parametric TC model sometimes exceed observed surges by over 100 cm (Figure 5(a)), while the error of surge predictions with MSM fields lies in the range of ±100 cm (Figure 5(b)). This suggests that surge prediction with MSM generally provides better prediction than with the parametric TC model.

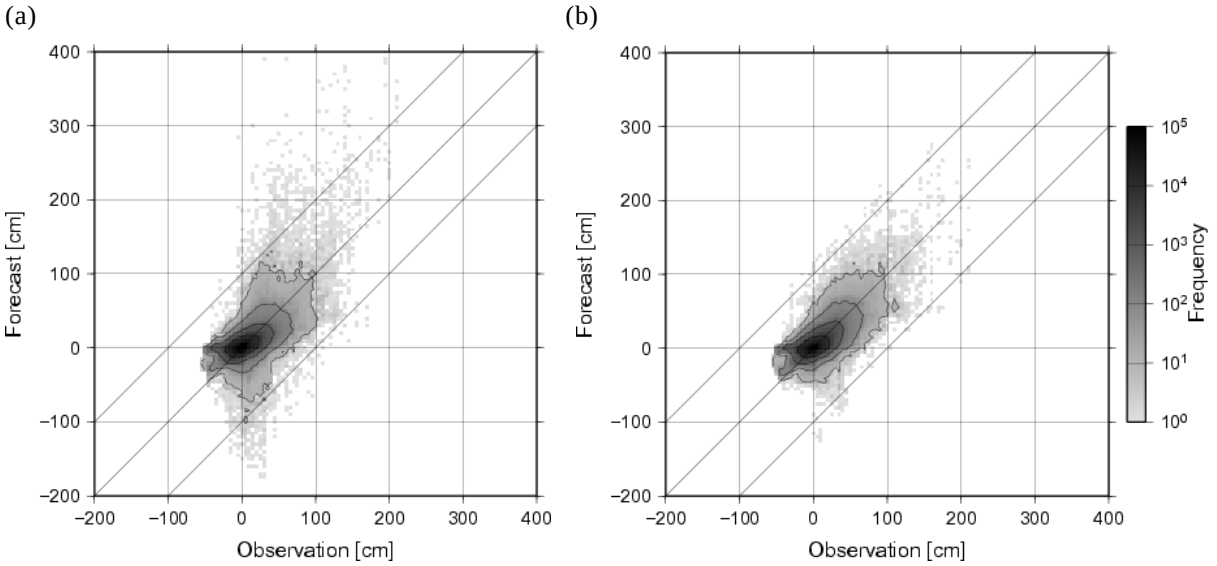

Figure 5　Scatter diagrams of predicted surges against the observed values.

(a) Predictions with parametric TC fields, (b) those with MSM.

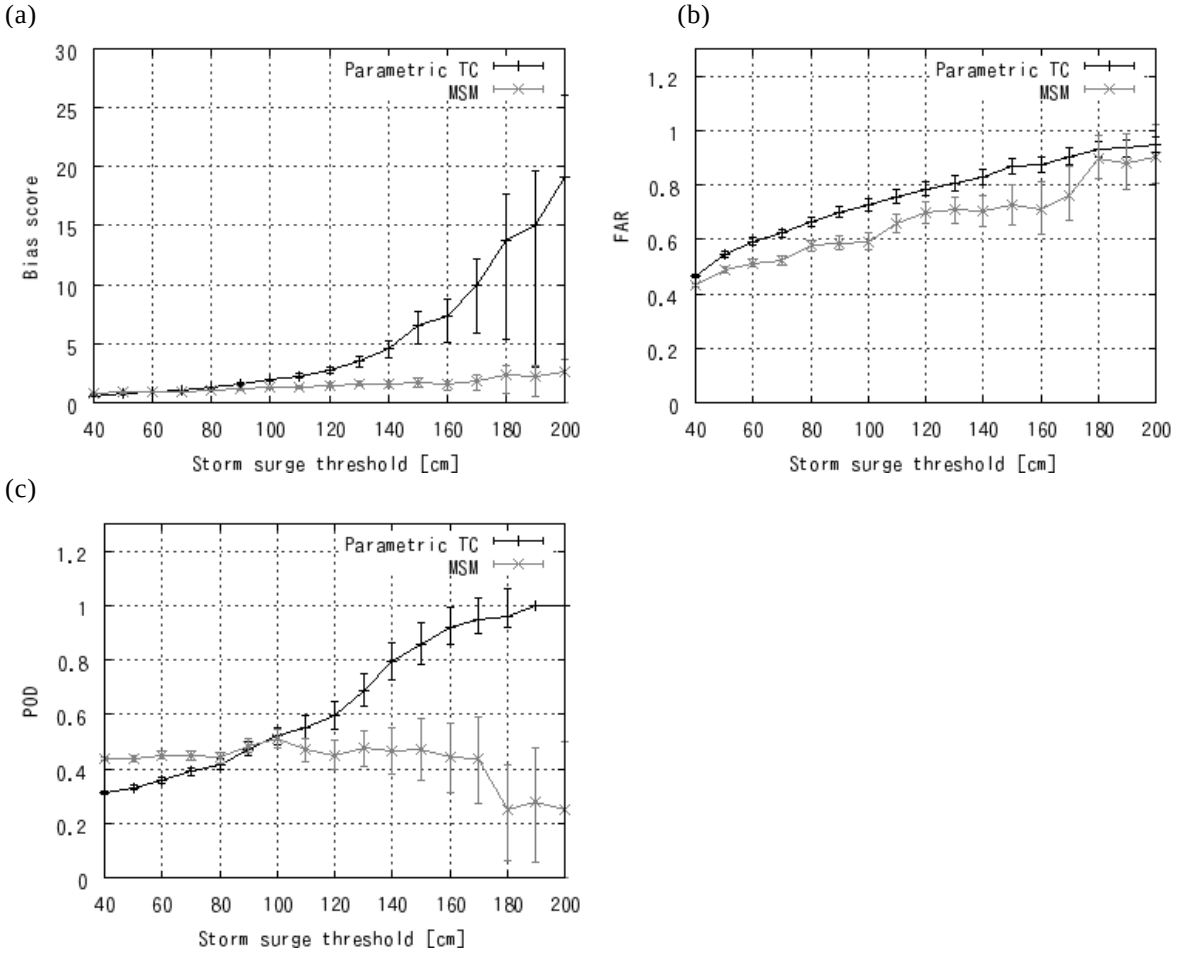

Figure 6　Verification scores.

(a) Bias score　(b) False alarm ratio (FAR)　(c) Probability of detection (POD).

To quantitatively evaluate the accuracy of the model, we also calculated verification scores; the bias score, the false alarm ratio (FAR) and the probability of detection (POD) (Figure 6). Refer to Appendix 2 for the definitions of these scores. The bias scores for the parametric TC model increase rapidly with the threshold, and those for storm surges of over one meter are much larger than one (the perfect score), while those of MSM are close to unity. The FAR scores increase with the threshold for both sets of predictions, but those for MSM are smaller than those of the parametric TC model. These two scores indicate that prediction with the parametric TC model has a tendency to overestimate, and that the use of MSM alleviates this tendency. On the other hand, for the threshold marking more than 100 cm, the POD of MSM is smaller than that for the parametric TC model, implying that prediction with MSM misses large storm surges more frequently than that with the parametric TC model. However, this is to be expected, since prediction with the parametric TC model has a tendency of overestimation as indicated by its large bias score.

In addition, to examine changes in accuracy with the forecast time, FAR and POD values for every six-hour period were calculated, and are shown in Figure 7. According to these figures, surge prediction with MSM gives better scores for short-range forecasts (FT=1 – 6), but its accuracy decreases with forecast time and approaches that of prediction with the parametric TC model after the 18-hour forecast point.

This comparative study suggests that the use of MSM will suppress the tendency of overestimation and improve the accuracy of short-range forecasting. Accordingly, we decided to use wind and pressure fields predicted by MSM as the forcing of the surge model as well as the parametric TC model, and have used this system since September 2007.

6. Summary and concluding remarks

This paper describes the major features of the operational storm surge prediction model at JMA. It is a two-dimensional model that runs eight times a day, providing 33-hour predictions of storm surges and sea levels for 290 points along the Japanese coast. The model results are used as the basis for storm surge warnings. One of its important features is that, when a TC is present around Japan, the model predicts multiple scenarios of storm surges with different meteorological forcing fields to allow for the uncertainty in TC track forecasts. A parametric TC model and JMA's nonhydrostatic mesoscale model are used as the sources of meteorological forcing for the storm surge model.

The performance of the storm surge model was investigated through two case studies and a comparative verification. Although the parametric TC model is useful for creating an ensemble of meteorological forcing, it was found to sometimes overestimate wind speed in TCs, resulting in overestimation in storm surge prediction. The results of the verification suggest that the use of MSM prediction for surge model forcing suppresses the tendency for overestimation and improves the short-range prediction of storm surges.

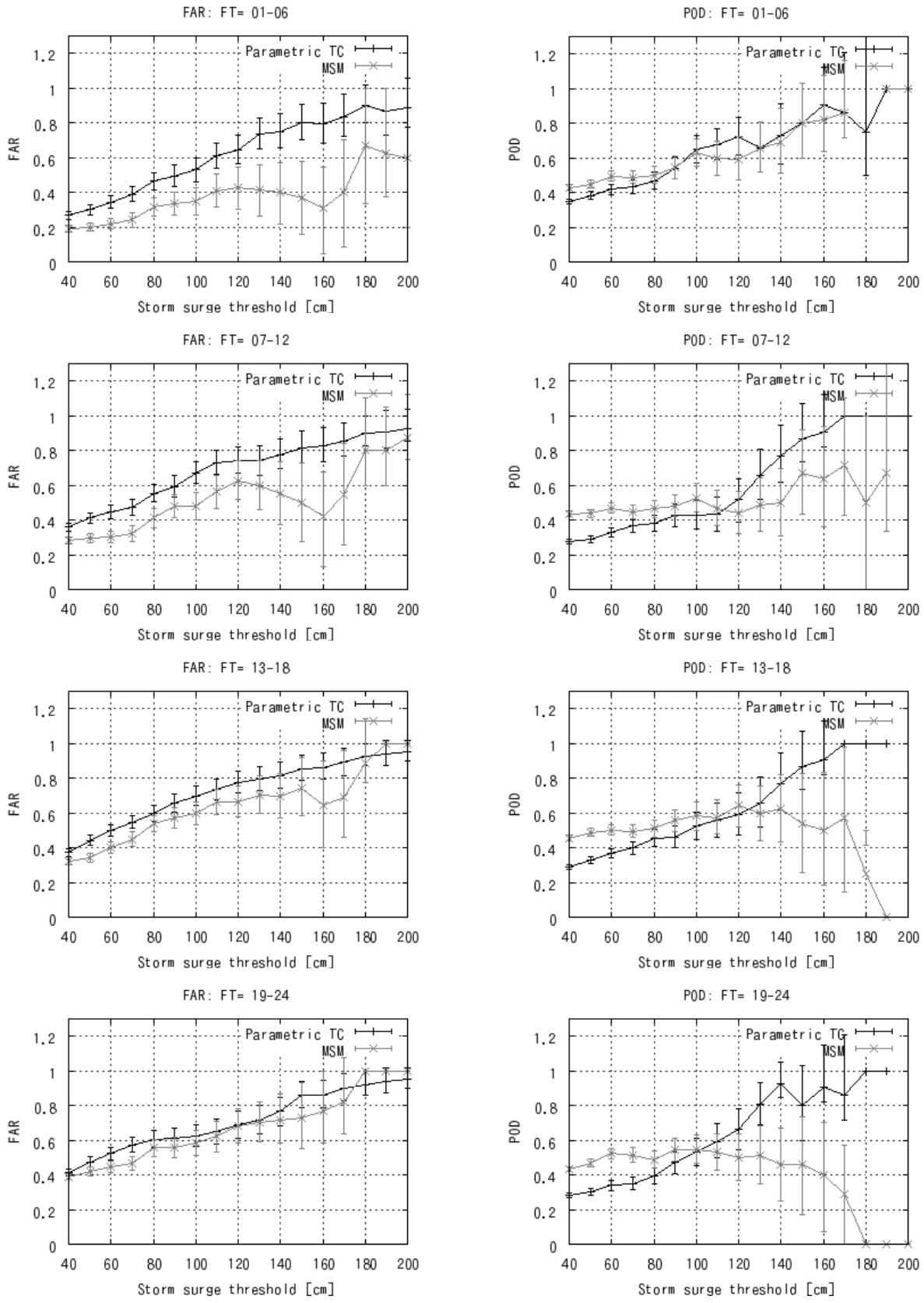

Figure 7　The false alarm ratio (left column) and probability of detection (right column) of the storm surge model for each six-hourly forecast period.

From top to bottom, scores for 1 – 6, 7 – 12, 13 – 18 and 19 – 24 hour forecasts, respectively.

As explained in Section 4, the model described in this paper calculates only storm surge components, but disaster mitigation activities also require astronomical tide prediction to forecast the total water level or storm tide. For this purpose, JMA carries out harmonic analysis of sea level data observed at tide stations for several to ten years, and calculates astronomical tides using the harmonic analysis results. This method gives pointwise astronomical tide predictions. In order to estimate astronomical tides at any given location without a tide station, JMA has been developing a data assimilation method to combine the information from observation data and an ocean tide model.

Storm surges are generally caused by wind setup and the inverted barometer effect. However, in addition to these effects, ocean waves also influence the occurrence of storm surges on coasts facing deep open seas; this effect is called *wave setup* (Longuet-Higgins and Stewart, 1964; Konishi, 1997). Since wave setup should also be predicted, but the current version of the JMA storm surge model does not consider it, a method to estimate its effects is now under development.

Lastly, the model computes water level changes at points in the sea, but the prediction of seawater inundation in coastal land areas remains beyond its scope.

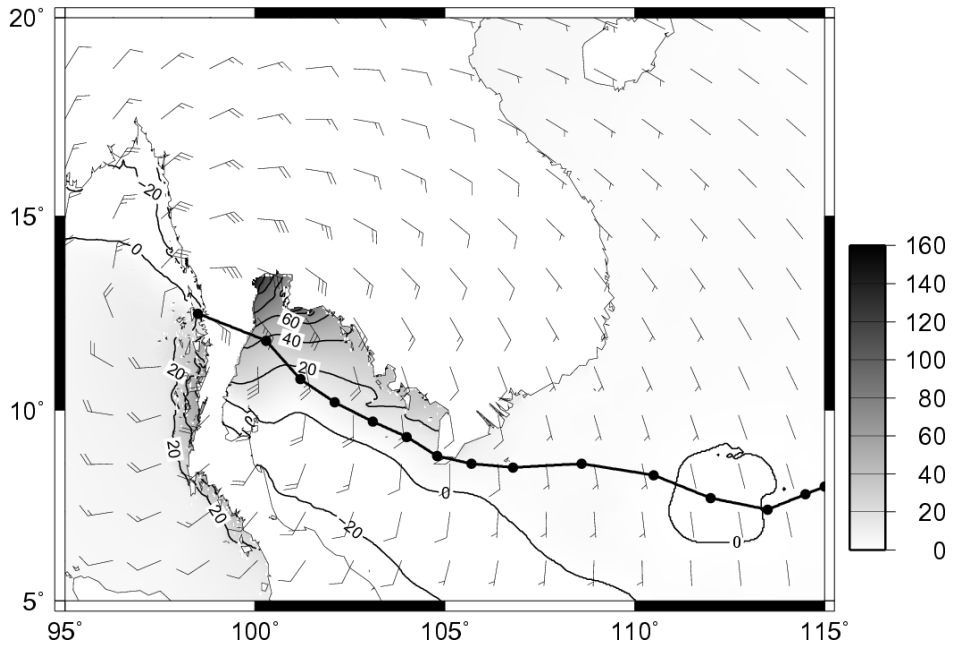

Figure A1 Modeled storm surge for the case of STS Linda (T9726).

The shaded areas show the modeled surge distribution for 00 UTC on 4 November 1997 (unit: cm).

The thick line represents the TC track, and the dots on the line depict the six-hourly positions.

Appendix 1 Application of the JMA storm surge model to storm surge events in Southeast Asia

Provided with appropriate sets of meteorological forcing fields and bathymetric data, this model can predict storm surges in countries other than Japan, and can be run on a PC if a modest model setting is chosen, such as a 2-arc-minute horizontal resolution and a 20°×20° model domain. As mentioned in Section 3, the input data needed are the TC parameters when the parametric TC model is used to create the external forcing of the surge model.

As an example of the model's application to surge events in Southeast Asia, its results for the surge event associated with STS Linda (T9726) are presented in Figure A1.

Appendix 2 Definitions of verification scores

This appendix gives the definitions of the verification scores used in this paper, which are based on Jolliffe and Stephenson (2003). All pairs of predicted and observed values are divided into four categories as shown in Table A1, and the frequencies of the four categories are used to calculate the verification scores.

Table A1 Contingency table

		Observed	
		Yes	No
Forecast	Yes	Hits	False alarms
	No	Misses	Correct negatives

(1) Bias score

The bias score is the ratio of the number of forecasts of occurrence to the number of actual occurrences. Scores range from 0 to infinity, and the perfect score is 1.

$$BS = \frac{(\text{hits}) + (\text{false alarms})}{(\text{hits}) + (\text{misses})} \qquad \text{(A1)}$$

(2) Probability of detection (POD)

This quantity is defined by:

$$POD = \frac{(\text{hits})}{(\text{hits}) + (\text{misses})} \qquad \text{(A2)}$$

It represents the total number of correct event forecasts (hits) divided by the total number of events observed. It ranges from 0 to 1, and the perfect score is 1.

(3) False alarm ratio (FAR)

FAR is defined by:

$$FAR = \frac{(\text{false alarms})}{(\text{hits}) + (\text{false alarms})} \qquad \text{(A3)}$$

It is the number of false alarms divided by the total number of event forecasts. It can vary from 0 to 1. A FAR value of zero represents perfect skill.

References

Fujita, T., 1952: “Pressure Distribution Within Typhoon”. *Geophys. Mag.*, **23**, 437-451.

Japan Meteorological Agency, 2008: Annual Report on Activities of the RSMC Tokyo - Typhoon Center. Available online at http://www.jma.go.jp/jma/jma-eng/jma-center/rsmc-hp-pub-eg/AnnualReport/2007/Text/Text2007.pdf

Jolliffe, I. T., and D. B. Stephenson, 2003: Forecast Verification: A Practitioner's Guide in Atmospheric Science, Wiley.

Konishi, T., 1995: An experimental storm surge prediction for the western part of the Inland Sea with application to Typhoon 9119. *Pap. Meteor. Geophys*., **46**, 9-17.

Konishi, T., 1997: A cause of storm surges generated at the ports facing open oceans – effect of wave setup –, *Umi to Sora (Sea and Sky)*, **73**, 35-44.

Longuet-Higgins, M. S., and R. W. Stewart, 1964: Radiation stress in water waves; a physical discussion, with applications. *Deep-Sea Research*, **11**, 529-562.

Saito, K., T. Fujita, Y. Yamada, J. Ishida, Y. Kumagai, K. Aranami, S. Ohmori, R. Nagasawa, S. Kumagai, C. Muroi, T. Kato, H. Eito and Y. Yamazaki, 2006: The operational JMA nonhydrostatic mesoscale model. *Mon. Wea. Rev*., **134**, 1266-1298.